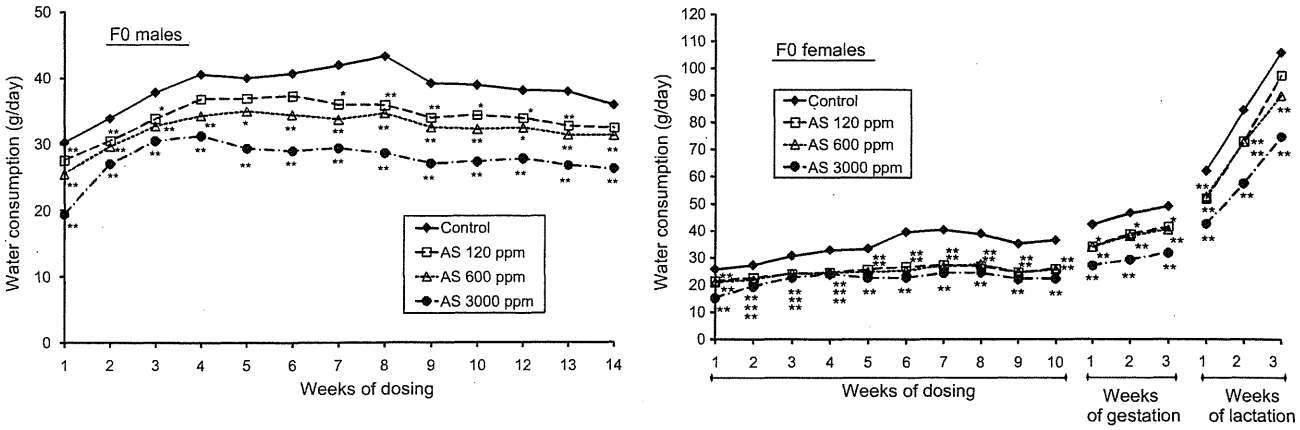

Fig. 1. Water consumption of F0 parental animals. *Significantly different from the control, $P < 0.05$, **significantly different from the control, $P < 0.01$.

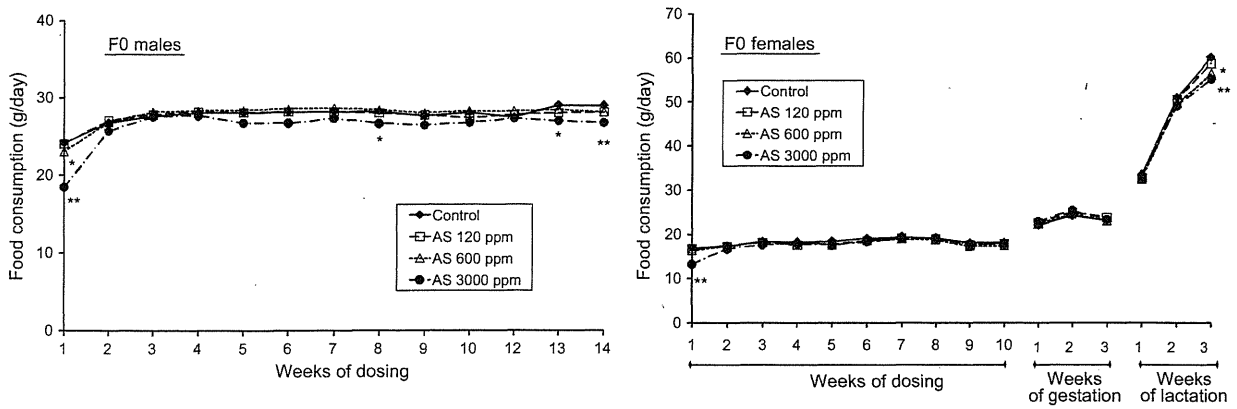

Fig. 2. Food consumption of F0 parental animals. *Significantly different from the control, $P < 0.05$, **significantly different from the control, $P < 0.01$.

control and 600 ppm groups (100 ± 0.0% versus 98.4 ± 7.3%). The surface righting reflex on PND 5 and negative geotaxis reflex on PND 8 were achieved in all male and female F2 pups in all groups, and no significant changes were found in the response time (data not shown).

As for the sexual development of F1 male and female animals, vaginal opening was significantly delayed at 3000 ppm (31.4 ± 1.7, compared to 29.5 ± 2.1 in control). At this dose, body weight at the time of vaginal opening was slightly heavier than the control (119.0 ± 13.3 g versus 109.6 ± 11.6 g) although not statistically significant. No significant differences between control and AS-treated groups were noted in the age at preputial separation or body weight at the time of completion in males.

3.4. Behavioral effects (F1)

Spontaneous locomotor activity at 10-min intervals and for 60 min was not significantly different between control and AS-treated groups in male and female F1 rats. In the water-filled *T*-maze test, pre-test swimming trials in the straight channel

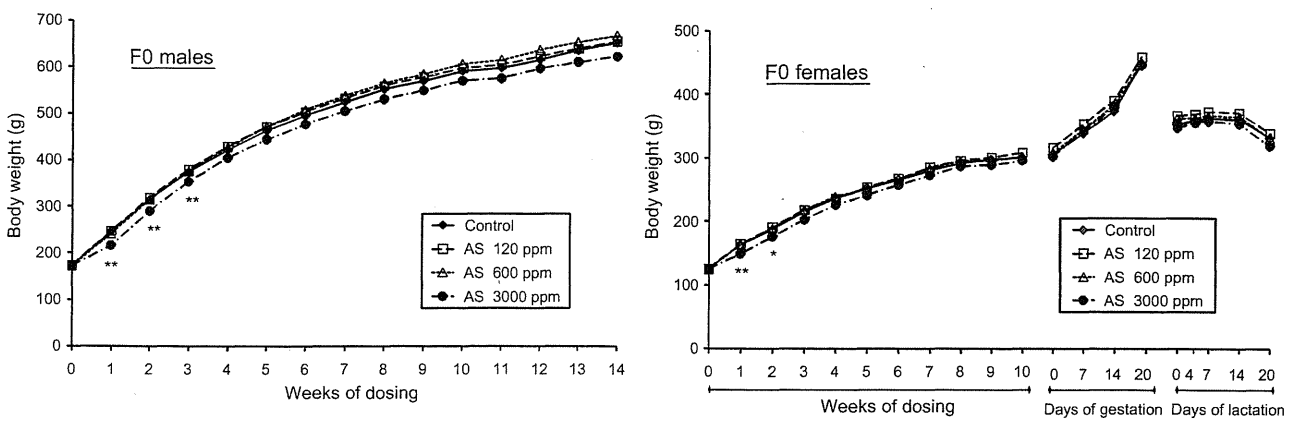

Fig. 3. Body weight of F0 parental animals. *Significantly different from the control, $P < 0.05$, **significantly different from the control, $P < 0.01$.

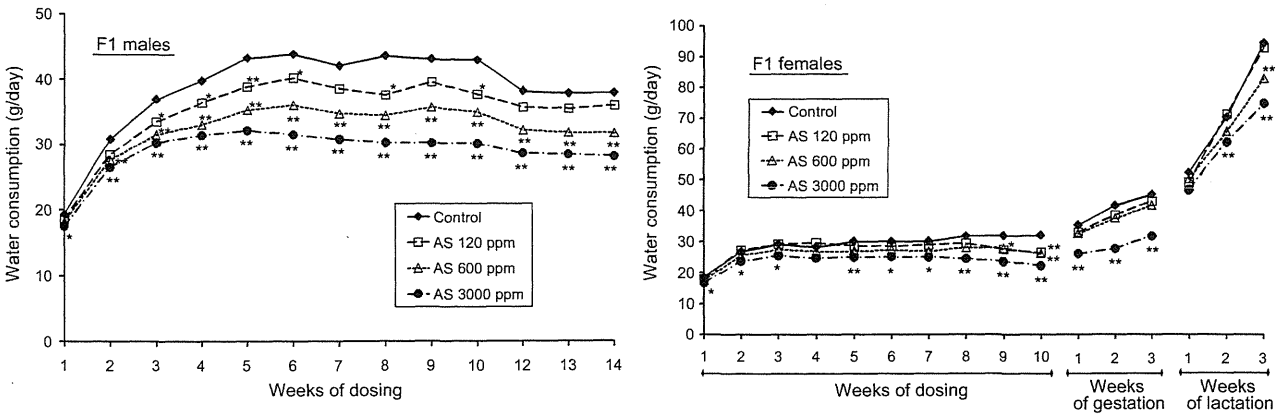

Fig. 4. Water consumption of F1 parental animals. *Significantly different from the control, $P < 0.05$, **significantly different from the control, $P < 0.01$.

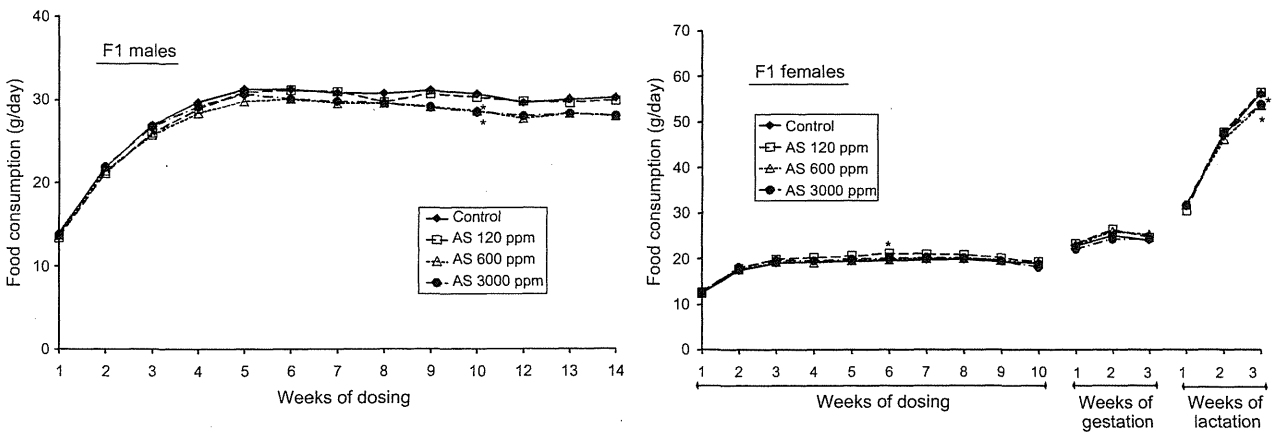

Fig. 5. Food consumption of F1 parental animals. *Significantly different from the control, $P < 0.05$, **significantly different from the control, $P < 0.01$.

revealed that all male and female F1 rats in each group could swim satisfactorily, and no significant changes were observed in the elapsed time to traverse the straight channel. On days 2–4 of the *T*-maze test, no significant changes were observed in the elapsed time and number of errors in males. In females, the elapsed time and the number of errors on day 2 of the *T*-maze was significantly lowered at 600 ppm, but there were no significant differences in the elapsed time or number of errors on days 3 and 4 of the *T*-maze test between control and AS-treated groups (data not shown).

3.5. Necropsy, organ weight and histopathology of adults (F0 and F1)

In F0 males, absolute and relative liver weights were significantly decreased at 3000 ppm. Absolute spleen weight was also

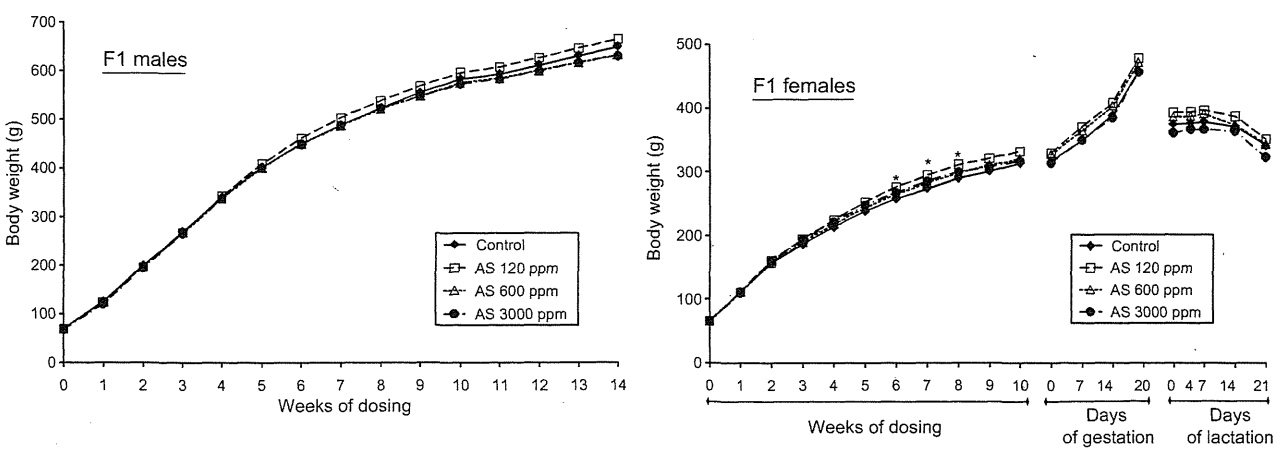

Fig. 6. Body weight of F1 parental animals. *Significantly different from the control, $P < 0.05$, **significantly different from the control, $P < 0.01$.

Table 1
Reproductive performance of F0 and F1 parental animals.

AS (ppm)		0 (control)	120	600	3000
F0 generation					
No. of rats (male/female)		24/24	24/24	24/24	24/24
Copulation index (%)[a]	Males	91.7	91.7	100	91.7
	Females	95.8	100	100	100
Precoital interval (days)[b]		3.2 ± 1.1	3.2 ± 1.8	2.9 ± 1.3	2.8 ± 1.6
Fertility index (%)[c]	Males	95.5	90.9	100	95.5
	Females	95.7	91.7	100	95.8
Gestation index (%)[d]		100	95.5	95.7	95.7
Gestation length (days)[b]		22.4 ± 0.5	22.5 ± 0.6	22.1 ± 0.4	22.3 ± 0.5
Delivery index (%)[b,e]		94.3 ± 5.6	88.6 ± 21.0	90.7 ± 20.8	92.0 ± 20.5
F1 generation					
No. of rats (male/female)		24/24	23/24	24/24	24/24
Copulation index (%)[a]	Males	95.8	91.3	95.8	87.5
	Females	100	95.8	100	95.8
Precoital interval (days)[b]		3.3 ± 3.2	3.0 ± 2.0	2.7 ± 1.5	2.3 ± 1.1
Fertility index (%)[c]	Males	91.3	81.0	91.3	95.2
	Females	91.7	82.6	91.7	91.3
Gestation index (%)[d]		100	94.7	100	100
Gestation length (days)[b]		22.4 ± 0.5	22.3 ± 0.5	22.2 ± 0.4	22.2 ± 0.4
Delivery index (%)[b,e]		94.0 ± 9.9	87.5 ± 22.6	91.4 ± 10.7	94.6 ± 6.8

[a] Copulation index (%) = (no. of animals with successful copulation/no. of animals paired) × 100.
[b] Values are given as the mean ± S.D.
[c] Fertility index (%) = (no. of animals that impregnated a female or were pregnant/no. of animals with successful copulation) × 100.
[d] Gestation index (%) = (no. of females that delivered live pups/no. of pregnant females) × 100.
[e] Delivery index (%) = (no. of pups delivered/no. of implantations) × 100.

decreased significantly in this group, but no significant change was found in the relative weight. In F1 males, the absolute weights of the adrenals at 3000 ppm and the testes at 600 ppm were significantly decreased without significant changes in the relative weight. There were no significant changes in the absolute and relative weights of any organ in F0 and F1 female adults (data not shown).

No dose-related gross lesions were found in F0 or F1 adults. Histopathological examination of the reproductive organs revealed no compound-related alterations. There was no significant difference in the number of primordial follicles in the ovary of F1 females between control and 3000 ppm groups (data not shown).

3.6. Necropsy, organ weight and histopathology of weanlings (F1 and F2)

Absolute and relative organ weights of male and female F1 weanlings are shown in Table 3. The 3000 ppm treated males and females had a significantly lower body weight at scheduled sacrifice than the controls. In this group, absolute and relative liver weights were significantly lower than the controls. Absolute spleen weight was also decreased significantly in both sexes of the 3000 ppm group, accompanied by a significant decrease in the relative weight in males. In addition, significant decreases in the absolute weight were found for the thymus in both sexes and for the kidneys, testes and epididymides in males at 3000 ppm, and for the uterus in females at 600 and 3000 ppm. Relative brain weight was significantly increased in both sexes of the 3000 ppm group.

Table 4 presents absolute and relative organ weights of male and female F2 weanlings. The mean body weight at scheduled sacrifice was significantly lowered in both sexes of the 3000 ppm group. In males, the absolute and relative weights of the thymus and spleen were significantly decreased in the 3000 ppm group. Significant decreases were also found in the absolute weight of the liver and epididymides at 3000 ppm. The relative brain weight was significantly increased at this dose. At 120 ppm, the only significant change was a non-dose-related decrease in the relative thymus weight. In F2 females, there were significant decreases in the absolute and relative weights of the liver, and the absolute weight of the spleen, ovary and uterus, and a significant increase in the relative brain weight at 3000 ppm. In addition, a significant decrease in the absolute brain weight was observed only in the 600 ppm group.

External and internal gross observations revealed no compound-related alterations either in F1 and F2 weanlings or in pups found dead during the preweaning period. There were no dose-related histopathological changes in the liver and spleen of male and female F1 and F2 weanlings.

4. Discussion

AS administered via the drinking water to male and female rats resulted in decreased water consumption for both sexes in all treatment groups. Since the dosing solution containing AS was pH 3.57–4.20, the acidity would decrease the palatability of drinking water in AS-treated groups. Decreased water consumption was associated with decreased food consumption by F0 and F1 males and females in the 600 and 3000 ppm groups and decreased body weight in F0 male and females in the 3000 ppm group. Since water-deprived animals typically reduce their levels of feed consumption and consequently lower their body weight [46], decreased food consumption and body weight observed in the present study could be considered secondary to the decreased water consumption. In the present study, food consumption and body weight fell notably during the early dosing period in F0 males and females. Food consumption also decreased in F0 and F1 females at the end of the lactation period, when F1 or F2 pups would commence eating and drinking for themselves [37]. Campbell et al. [46] reported that animals have a certain amount of "buffering" capacity in the form of physiological mechanisms acting to reduce fluid loss. This might explain notable changes around the time when rats start drinking AS-containing water.

Continuous drinking of AS-contained water for two generations did not result in changes in copulation, fertility or gestation indices, pre-coital or gestation length, the number of implantations or pups delivered, or the incidence of pups with malformations or variations. In addition, adverse effects were not found in estrous cyclicity or sperm parameters, and the histopathology of reproductive tissues in male and female parental animals. Previous studies have demonstrated that parenterally administered aluminium affected

Table 2
Sex ratio, viability and body weight for F1 and F2 pups.

AS (ppm)	0 (control)	120	600	3000
F1 offspring				
No. of litters	22	21	22	22
No. of pups delivered[a]	13.9 ± 1.7	12.4 ± 4.7	13.1 ± 4.1	13.1 ± 3.4
Sex ratio of pups[b]	0.503	0.462	0.513	0.536
Viability index of pups (%)[a]				
On PND 0[c]	100.0 ± 0.0	99.3 ± 2.3	99.7 ± 1.6	99.5 ± 2.4
On PND 4[d]	98.7 ± 2.9	95.2 ± 21.8	98.8 ± 2.6	98.0 ± 5.4
On PND 21[e]	99.4 ± 2.7	100.0 ± 0.0	100.0 ± 0.0	99.4 ± 2.7
Male pup weight during lactation (g)[a]				
On PND 0	7.05 ± 0.61	7.25 ± 0.99	6.74 ± 0.69	6.96 ± 0.76
On PND 4	11.04 ± 0.85	11.41 ± 1.99	10.86 ± 1.37	11.00 ± 1.06
On PND 7	18.91 ± 1.29	19.36 ± 2.77	18.59 ± 1.71	18.47 ± 1.35
On PND 14	37.70 ± 2.63	37.97 ± 3.08	37.39 ± 2.59	36.34 ± 2.41
On PND 21	62.48 ± 4.50	62.63 ± 6.14	60.77 ± 4.01	57.34 ± 4.86**
Female pup weight during lactation (g)[a]				
On PND 0	6.61 ± 0.55	6.89 ± 0.83	6.35 ± 0.57	6.60 ± 0.64
On PND 4	10.46 ± 0.89	11.06 ± 1.71	10.27 ± 1.33	10.43 ± 0.83
On PND 7	18.03 ± 1.27	18.56 ± 2.31	17.69 ± 1.61	17.61 ± 1.21
On PND 14	36.29 ± 2.71	36.94 ± 3.03	35.67 ± 2.60	35.31 ± 2.24
On PND 21	60.17 ± 4.16	60.87 ± 5.68	57.68 ± 4.33	55.60 ± 4.34**
F2 offspring				
No. of litters	22	18	22	21
No. of pups delivered[a]	13.1 ± 3.6	13.2 ± 3.8	12.6 ± 3.9	14.0 ± 1.9
Sex ratio of pups[b]	0.528	0.502	0.536	0.457
Viability index of pups (%)[a]				
On PND 0[c]	99.68 ± 1.51	99.49 ± 2.14	98.42 ± 3.57	98.69 ± 3.60
On PND 4[d]	94.72 ± 14.54	98.07 ± 5.45	99.07 ± 3.15	99.01 ± 2.49
On PND 21[e]	100.00 ± 0.00	98.61 ± 4.04	100.00 ± 0.00	100.00 ± 0.00
Male pup weight during lactation (g)[a]				
On PND 0	6.97 ± 0.68	6.92 ± 0.81	6.87 ± 0.74	6.89 ± 0.60
On PND 4	10.73 ± 1.62	10.53 ± 1.27	11.27 ± 1.81	10.52 ± 1.15
On PND 7	17.96 ± 2.05	17.51 ± 2.12	18.83 ± 2.39	17.72 ± 1.60
On PND 14	35.79 ± 3.52	36.18 ± 3.63	37.32 ± 4.15	35.44 ± 2.73
On PND 21	59.61 ± 5.45	59.44 ± 5.67	60.12 ± 7.12	56.36 ± 4.47
Female pup weight during lactation (g)[a]				
On PND 0	6.66 ± 0.69	6.38 ± 0.78	6.41 ± 0.65	6.50 ± 0.49
On PND 4	10.22 ± 1.63	9.70 ± 1.23	10.36 ± 1.54	9.98 ± 0.91
On PND 7	17.03 ± 1.99	16.36 ± 2.35	17.40 ± 2.18	16.89 ± 1.23
On PND 14	34.82 ± 3.52	34.17 ± 3.58	34.96 ± 4.24	34.01 ± 2.09
On PND 21	57.33 ± 4.90	56.11 ± 5.54	56.41 ± 6.04	54.16 ± 2.82*

[a] Values are given as the mean ± S.D.
[b] Sex ratio = total no. of male pups/total no. of pups.
[c] Viability index on PND 0 (%) = (no. of live pups on PND 0/no. of pups delivered) × 100.
[d] Viability index on PND 4 (%) = (no. of live pups on PND 4/no. of live pups on PND 0) × 100.
[e] Viability index on PND 21 (%) = (no. of live pups on PND 21/no. of live pups on PND 4 after cull) × 100.
* Significantly different from the control, $P < 0.05$.
** Significantly different from the control, $P < 0.01$.

male reproductive systems, causing decreases in testicular and epididymal sperm counts, necrosis of spermatocytes/spermatids in the testes, and reduction of fertility, etc., in rats and mice [19,20,47]. Although aluminium has extremely low oral bioavailability (less than 1%) [48,49], male reproductive toxicity was also observed in oral gavage studies [22,23,50]. In the 6-month oral gavage study in rats, changes in the number of spermatozoa and motility, and the substantial proliferation of interstitial cells in the testes were observed at doses as low as 2.5 mg Al/kg/day (as aluminium chloride) [50]. The primary reason why such effects were not detected in the present study might be a difference in the administration method because the toxicokinetic behavior of chemicals given as a bolus dose by gavage must differ significantly from those after continuous administration via drinking water. Another possible factor is aluminium content in the laboratory animal feed, for which substantial brand-to-brand and lot-to-lot variations, ranging from 60 to 8300 ppm, have been reported [51]. Since the dietary intake of aluminium was not considered in these oral gavage studies, toxic effects of aluminium could be overestimated. As for continuous exposure studies, taking into account the aluminium content in the basal diet, Hicks et al. [52] demonstrated that 28-day continuous dietary exposure to basic sodium aluminium phosphate or aluminium hydroxide did not affect the testicular histopathology up to 302 mg Al/kg/day in Sprague–Dawley rats. In the 26-week feeding study of basic sodium aluminium phosphate in beagle dogs, germinal epithelial cell degeneration and atrophy in the seminiferous tubules were observed at 75 mg Al/kg bw/day [21], but such effects on male reproductive organs were not detected up to 88 mg Al/kg/day in the similar subchronic dietary study for acidic sodium aluminium phosphate in beagle dogs [53]. These dietary studies used water-insoluble or sparingly soluble forms of aluminium [8,51]. Since it is widely assumed that insoluble aluminium compounds are less bioavailable than soluble compounds, such as AS, aluminium chloride and aluminium lactate [8], there is a possibility that the male reproductive toxicity of aluminium was underestimated in these previous dietary exposure studies. The present two-generation study provided useful information that the male reproductive system is not affected even after continuous exposure to a water-soluble aluminium compound, at least up to around 50 mg Al/kg bw/day.

In the present study, some developmental effects were observed. Male and female F1 pups and female F2 pups in the

Table 3
Absolute and relative organ weight of F1 male and female weanlings.

AS (ppm)		0 (control)	120	600	3000
Males					
No. of animals		22	20	22	22
Body weight	(g)	90.8 ± 6.9	93.4 ± 10.5	89.7 ± 6.1	79.4 ± 7.5**
Brain	(g)	1.69 ± 0.06	1.73 ± 0.08	1.72 ± 0.07	1.68 ± 0.05
	(g/100 g bw)	1.88 ± 0.13	1.87 ± 0.19	1.92 ± 0.09	2.14 ± 0.17**
Thymus	(mg)	375 ± 55	384 ± 86	357 ± 58	305 ± 51**
	(mg/100 g bw)	414 ± 56	409 ± 64	398 ± 59	383 ± 36
Liver	(g)	4.33 ± 0.43	4.40 ± 0.60	4.22 ± 0.45	3.49 ± 0.53**
	(g/100 g bw)	4.77 ± 0.30	4.71 ± 0.33	4.70 ± 0.27	4.37 ± 0.30**
Kidney[a]	(g)	1.06 ± 0.09	1.09 ± 0.14	1.03 ± 0.11	0.95 ± 0.13**
	(g/100 g bw)	1.17 ± 0.06	1.16 ± 0.07	1.15 ± 0.08	1.20 ± 0.07
Spleen	(mg)	394 ± 49	410 ± 68	388 ± 74	301 ± 43**
	(mg/100 g bw)	436 ± 63	437 ± 40	432 ± 73	379 ± 37**
Testis[a]	(mg)	596 ± 65	583 ± 67	569 ± 65	539 ± 51*
	(mg/100 g bw)	657 ± 64	626 ± 49	635 ± 64	682 ± 58
Epididymis[a]	(mg)	81.8 ± 8.6	76.8 ± 10.9	76.5 ± 8.4	72.0 ± 9.9**
	(mg/100 g bw)	90.4 ± 10.3	82.0 ± 6.1	85.4 ± 8.4	91.5 ± 14.6
Females					
No. of animals		22	20	22	21
Body weight	(g)	84.3 ± 6.3	85.9 ± 9.2	80.5 ± 7.0	75.8 ± 6.4**
Brain	(g)	1.64 ± 0.06	1.66 ± 0.06	1.63 ± 0.05	1.63 ± 0.07
	(g/100 g bw)	1.96 ± 0.12	1.95 ± 0.18	2.04 ± 0.17	2.16 ± 0.14**
Thymus	(mg)	383 ± 66	373 ± 74	345 ± 46	313 ± 33**
	(mg/100 g bw)	453 ± 63	433 ± 64	429 ± 57	415 ± 41
Liver	(g)	3.83 ± 0.47	3.92 ± 0.48	3.61 ± 0.35	3.24 ± 0.34**
	(g/100 g bw)	4.53 ± 0.30	4.57 ± 0.31	4.48 ± 0.30	4.27 ± 0.25*
Kidney[a]	(g)	0.99 ± 0.11	0.99 ± 0.09	0.93 ± 0.10	0.93 ± 0.10
	(g/100 g bw)	1.17 ± 0.08	1.15 ± 0.07	1.15 ± 0.09	1.23 ± 0.09
Spleen	(mg)	337 ± 62	356 ± 55	341 ± 64	292 ± 43*
	(mg/100 g bw)	400 ± 67	415 ± 44	422 ± 53	386 ± 47
Ovary[a]	(mg)	25.3 ± 4.8	25.3 ± 3.8	22.5 ± 4.6	24.7 ± 3.2
	(mg/100 g bw)	30.1 ± 5.1	29.7 ± 5.0	27.9 ± 5.0	32.5 ± 4.2
Uterus	(mg)	70.6 ± 16.6	74.2 ± 32.0	59.2 ± 11.9*	55.4 ± 13.4**
	(mg/100 g bw)	83.8 ± 19.2	85.5 ± 32.4	73.3 ± 11.9	73.3 ± 18.0

Values are given as the mean ± S.D.
[a] Values represent the total weights of the organs on both sides.
* Significantly different from the control, $P < 0.05$.
** Significantly different from the control, $P < 0.01$.

3000 ppm group had a lower body weight on PND 21 while no difference was found in the birth weight. Such inhibition of the preweaning body weight gain may be simply attributable to the decreased palatability of the drinking water, which would decrease the water intake of pups themselves or might decrease the amount of maternal breast milk; however, similar developmental effects of aluminium were reported in the previous three dietary exposure studies, in which aluminium lactate was mixed in the diet and fed to mice from day 0 of gestation throughout the lactation period [28,30,32], and the lowest effect level was 500 ppm, which was estimated to be equal to 94–273 mg Al/kg bw/day based on the body weight and food consumption during the lactation period [28]. In these dietary exposure studies, food consumption was decreased, but Golub et al. [28] indicated that the mean body weight of pups on PNDs 15 and 20 in the 1000 ppm group was lower than that of the pair-fed control. In contrast, the effects on body weight of preweaning mice were not found in the other two dietary exposure studies [29,31], which were conducted using a similar study design by the same research group. Donald et al. [29] discussed differences in the constituents of the diet as a possible cause of the inconsistent results, but this speculation appears to be contradicted by a subsequent study [30]. Although it is still unclear why different results were obtained in these dietary exposure studies, these results suggest that the fall in body weight around weaning in the present study might not be explained only by decreased water intake. Aluminium ingested by pups themselves and/or taken via maternal milk may affect preweaning growth, or impairment of maternal nursing behavior or the lactation status could be considered possible factors.

In F1 and F2 weanlings, various organ weight changes were found in the 3000 ppm group. Among them, an increase in the relative brain weight is considered to be a secondary change that occurs with the fall in body weight because the absolute weight did not change. Similarly, decreased absolute weights of the kidneys, testes, epididymides, uterus, etc., without changes in the relative weight, were thought to be associated with decreased body weight. On the other hand, the effects on the liver and spleen, the absolute and relative weights of which were decreased in both generations, could not be explained only by the fall of body weight. Since similar effects were observed in the above-mentioned dietary exposure study of aluminium lactate [28], the effects on the liver and spleen weight might be a direct effect of aluminium ingested by pups themselves and/or taken via maternal milk; however, in the present study, no histopathological changes were detected in the liver and spleen. Furthermore, the changes in the liver or spleen weight were not detected in adults, except for F0 males in the 3000 ppm group; therefore, organ weight changes observed in F1 and F2 weanlings in the 3000 ppm group were not deemed to be adverse effects. Organ weight changes in the 120 and 600 ppm groups were not considered to have toxicological significance because these changes were not dose-dependent or were inconsistent across generations.

As for effects on the developmental landmarks, vaginal opening was slightly delayed in F1 females in the 3000 ppm group while no compound-related changes were found in the other developmental landmarks, including male preputial separation. Vaginal opening generally occurs around the time of first ovulation in response to an increase in serum estradiol levels as females enter puberty [54], and therefore, it is widely used as a marker of female puberty.

Table 4
Absolute and relative organ weight of F2 male and female weanlings.

AS (ppm)		0 (control)	120	600	3000
Males					
No. of animals		21	18	22	21
Body weight	(g)	87.7 ± 5.8	89.0 ± 8.7	87.0 ± 9.6	79.2 ± 6.8**
Brain	(g)	1.66 ± 0.05	1.69 ± 0.06	1.70 ± 0.06	1.67 ± 0.06
	(g/100 g bw)	1.90 ± 0.13	1.91 ± 0.17	1.97 ± 0.16	2.13 ± 0.17**
Thymus	(mg)	382 ± 50	348 ± 49	357 ± 66	305 ± 36**
	(mg/100 g bw)	439 ± 70	392 ± 52*	411 ± 57	386 ± 40**
Liver	(g)	3.93 ± 0.37	4.04 ± 0.64	3.91 ± 0.39	3.45 ± 0.41**
	(g/100 g bw)	4.49 ± 0.34	4.52 ± 0.44	4.50 ± 0.24	4.36 ± 0.23
Kidney[a]	(g)	1.02 ± 0.09	1.01 ± 0.13	0.99 ± 0.13	0.94 ± 0.10
	(g/100 g bw)	1.16 ± 0.08	1.14 ± 0.06	1.14 ± 0.07	1.19 ± 0.06
Spleen	(mg)	368 ± 54	381 ± 62	361 ± 49	296 ± 48**
	(mg/100 g bw)	421 ± 64	427 ± 50	416 ± 48	372 ± 42**
Testis[a]	(mg)	559 ± 67	549 ± 98	543 ± 77	534 ± 54
	(mg/100 g bw)	637 ± 60	615 ± 81	624 ± 47	680 ± 92
Epididymis[a]	(mg)	75.3 ± 6.9	78.3 ± 8.8	75.1 ± 10.7	70.5 ± 5.7*
	(mg/100 g bw)	86.1 ± 8.3	88.4 ± 9.0	86.5 ± 9.0	89.4 ± 8.2
Females					
No. of animals		22	18	21	21
Body weight	(g)	80.8 ± 6.0	80.0 ± 7.2	80.8 ± 9.1	73.8 ± 4.4**
Brain	(g)	1.60 ± 0.06	1.61 ± 0.05	1.64 ± 0.05*	1.61 ± 0.04
	(g/100 g bw)	1.99 ± 0.14	2.03 ± 0.16	2.05 ± 0.20	2.19 ± 0.15**
Thymus	(mg)	337 ± 45	364 ± 36	347 ± 49	312 ± 37
	(mg/100 g bw)	419 ± 61	457 ± 50	431 ± 47	424 ± 54
Liver	(g)	3.56 ± 0.35	3.61 ± 0.39	3.61 ± 0.48	3.07 ± 0.26**
	(g/100 g bw)	4.41 ± 0.21	4.51 ± 0.26	4.47 ± 0.26	4.17 ± 0.29**
Kidney[a]	(g)	0.95 ± 0.07	0.93 ± 0.10	0.92 ± 0.10	0.88 ± 0.08
	(g/100 g bw)	1.18 ± 0.08	1.16 ± 0.09	1.14 ± 0.06	1.20 ± 0.07
Spleen	(mg)	320.9 ± 46.7	331.8 ± 59.3	331.3 ± 57.1	269.9 ± 55.2**
	(mg/100 g bw)	398.4 ± 59.0	414.8 ± 64.3	409.0 ± 42.2	365.0 ± 67.4
Ovary[a]	(mg)	23.9 ± 3.7	22.8 ± 3.6	23.2 ± 3.5	20.2 ± 2.3**
	(mg/100 g bw)	29.7 ± 4.9	28.8 ± 5.6	29.0 ± 4.7	27.5 ± 3.5
Uterus	(mg)	60.5 ± 17.0	63.8 ± 18.4	65.0 ± 41.7	49.3 ± 11.6*
	(mg/100 g bw)	74.6 ± 19.2	79.3 ± 19.3	78.7 ± 40.4	67.0 ± 16.2

Values are given as the mean ± S.D.
[a] Values represent the total weights of the organs on both sides.
* Significantly different from the control, $P < 0.05$.
** Significantly different from the control, $P < 0.01$.

On the other hand, vaginal opening is closely related to body weight, and growth retardation can delay the day of acquisition [55]. In the present study, body weight at the time of vaginal opening was slightly heavier in F1 females of the highest dose group, compared with the control. However, other hormone-dependent events, including estrous cyclicity and AGD, were not changed in AS-treated groups. It seems unlikely that aluminium have a clear impact on the hormonal event. Further studies are required to draw a definitive conclusion on the effects of aluminium on the sexual maturation.

Aluminium has been reported to affect the developing nervous system [56,57]. In continuous exposure studies using rodents, the neurobehavioral effects were reported as follows: dietary exposure of pregnant rats to aluminium chloride or lactate at more than 96 mg Al/kg bw/day impaired the righting reflex, gasping reflex, negative geotaxis and/or locomotor coordination of preweaning pups [25,26]. Impaired performance of operant conditioning tasks, accompanied by a decrease in locomotor activity, was observed on PND 65 in the offspring of rats receiving a diet containing aluminium lactate at 400 mg Al/kg bw/day during gestation [58], suggesting that the effects continue after maturation. Unfortunately, aluminium concentration in the basal diet was not reported in these feeding studies using rats. Similar neurobehavioral effects were found in the preweaning, juvenile and adult periods of the offspring after dietary exposure of mice to aluminium lactate throughout the gestation and lactation periods [28–32]. These mouse studies took the basal diet content of the aluminium diet into consideration, and the lowest observed effect level was 500 ppm, corresponding to 100 mg Al/kg bw/day at the beginning of pregnancy and 210 mg Al/kg/day near the end of lactation [29]. In the present study, no changes were found in the reflex ontogeny of F1 and F2 pups and in spontaneous locomotor activity tested at 4 weeks of age for F1 animals. As for the performance in a water-filled multiple *T*-maze, a transient decrease in the elapsed time and the number of errors were found in F1 females in the 600 ppm group, but this change was not considered to be treatment-related because of the lack of dose-dependency. These findings indicate that previous findings of developmental neurotoxic effects were possibly related to the toxic effects of aluminium given at higher doses than those given in this study.

In summary, AS administered via drinking water at 120, 600 or 3000 ppm resulted in decreased water consumption. This change was associated with decreased food consumption in the 600 and 3000 ppm groups and decreased body weight in the 3000 ppm group. In the 3000 ppm group, male and female pups had a lower body weight on PND 21. At this dose, vaginal opening was slightly delayed. No definitive effects were found in the other reproductive/developmental parameters, including developmental neurobehavioral toxicity. Although there is a possibility that observed developmental effects are results of decreased water consumption, more definitive conclusions could not be reached since paired-comparison data are not available to assess the effects of decreased water intake in the absence of AS exposure. Based on these considerations, a conservative evaluation of the data led to the conclusion that the no observed adverse effect level of AS in this two-generation study is 600 ppm (41.0 mg/kg bw/day) for parental systemic toxicity and reproductive/developmental toxicity. The total ingested dose of aluminium from food and drinking

water combined in this 600 ppm group was calculated to be 8.06 mg Al/kg bw/day.

Conflict of interest statement

The authors declare that there are no conflicts of interest.

Acknowledgement

This study was supported by the Ministry of Health, Labour and Welfare, Japan.

References

[1] IPCS (International Programme on Chemical Safety). Aluminium. Environmental health criteria, vol. 194. Geneva: World Health Organization; 1997.
[2] Lantzy RJ, Fred TM. Atmospheric trace metals: global cycles and assessment of man's impact. Geochim Cosmochim Acta 1979;43:511–25.
[3] Hjortsberg U, Orbaek P, Arborelius Jr M, Karlsson JE. Upper airway irritation and small airways hyperreactivity due to exposure to potassium aluminium tetrafluoride flux: an extended case report. Occup Environ Med 1994;51:706–9.
[4] Jederlinic PJ, Abraham JL, Churg A, Himmelstein JS, Epler GR, Gaensler EA. Pulmonary fibrosis in aluminum oxide workers. Investigation of nine workers, with pathologic examination and microanalysis in three of them. Am Rev Respir Dis 1990;142:1179–84.
[5] Sjogren B, Lidums V, Hakansson M, Hedstrom L. Exposure and urinary excretion of aluminum during welding. Scand J Work Environ Health 1985;11:39–43.
[6] Shore D, Wyatt RJ. Aluminum and Alzheimer's disease. J Nerv Ment Dis 1983;171:553–8.
[7] Lione A. The prophylactic reduction of aluminium intake. Food Chem Toxicol 1983;21:103–9.
[8] IPCS (International Programme on Chemical Safety). Aluminium from all sources, including food additives (addendum). In: Safety evaluation of certain food additives and contaminants, prepared by the sixty-seventh meeting of the Joint FAO/WHO Expert Committee on Food Additives (JECFA), WHO food additives series 58. Geneva: Organization WH; 2007. p. 119–208.
[9] WHO (World Health Organization). 12.5 Aluminium. Guidelines for drinking-water quality: incorporating the first and second addenda, vol. 1 recommendations, 3rd ed. Geneva: World Health Organization; 2008. p. 301–3.
[10] Goyer RA, Clarkson JW. Toxic effects of metals. In: Klaassen CD, editor. Casarett and Doull's toxicology: the basic science of poisons. 6th ed. New York: McGraw-Hill; 2001. p. 811–67.
[11] Kerr DNS, Ward MK, Ellis HA, Simpson W, Parkinson IS. Aluminium intoxication in renal disease. In: Chadwick DJ, Whelan J, editors. Aluminium in biology and medicine (Ciba Foundation Symposium). Chihcester: Wiley; 1992. p. 123–41.
[12] Rondeau V. A review of epidemiologic studies on aluminum and silica in relation to Alzheimer's disease and associated disorders. Rev Environ Health 2002;17:107–21.
[13] Jansson ET. Aluminum exposure and Alzheimer's disease. J Alzheimers Dis 2001;3:541–9.
[14] Flaten TP. Aluminium as a risk factor in Alzheimer's disease, with emphasis on drinking water. Brain Res Bull 2001;55:187–96.
[15] Golub MS, Donald JM, Gershwin ME, Keen CL. Effects of aluminum ingestion on spontaneous motor activity of mice. Neurotoxicol Teratol 1989;11:231–5.
[16] Petit TL, Biederman GB, McMullen PA. Neurofibrillary degeneration, dendritic dying back, and learning-memory deficits after aluminum administration: implications for brain aging. Exp Neurol 1980;67:152–62.
[17] Lipman JJ, Colowick SP, Lawrence PL, Abumrad NN. Aluminum induced encephalopathy in the rat. Life Sci 1988;42:863–75.
[18] Strong MJ, Garruto RM. Chronic aluminum-induced motor neuron degeneration: clinical, neuropathological and molecular biological aspects. Can J Neurol Sci 1991;18:428–31.
[19] Llobet JM, Colomina MT, Sirvent JJ, Domingo JL, Corbella J. Reproductive toxicology of aluminum in male mice. Fundam Appl Toxicol 1995;25:45–51.
[20] Guo CH, Lu YF, Hsu GSH. The influence of aluminium exposure on male reproduction and offspring in mice. Environ Toxicol Pharmacol 2005;20:135–41.
[21] Pettersen JC, Hackett DS, Zwicker GM, Sprague GL. Twenty-six week toxicity study with KASAL (basic sodium aluminium phosphate) in beagle dogs. Environ Geochem Health 1990;12:121–3.
[22] Yousef MI, El-Morsy AM, Hassan MS. Aluminium-induced deterioration in reproductive performance and seminal plasma biochemistry of male rabbits: protective role of ascorbic acid. Toxicology 2005;215:97–107.
[23] Roy AK, Talukder G, Sharma A. Similar effects in vivo of two aluminum salts on the liver, kidney, bone, and brain of *Rattus norvegicus*. Bull Environ Contam Toxicol 1991;47:288–95.
[24] Paternain JL, Domingo JL, Llobet JM, Corbella J. Embryotoxic and teratogenic effects of aluminum nitrate in rats upon oral administration. Teratology 1988;38:253–7.
[25] Bernuzzi V, Desor D, Lehr PR. Effects of prenatal aluminum exposure on neuromotor maturation in the rat. Neurobehav Toxicol Teratol 1986;8:115–9.
[26] Bernuzzi V, Desor D, Lehr PR. Developmental alternations in offspring of female rats orally intoxicated by aluminum chloride or lactate during gestation. Teratology 1989;40:21–7.
[27] Domingo JL, Paternain JL, Llobet JM, Corbella J. Effects of oral aluminum administration on perinatal and postnatal development in rats. Res Commun Chem Pathol Pharmacol 1987;57:129–32.
[28] Golub MS, Gershwin ME, Donald JM, Negri S, Keen CL. Maternal and developmental toxicity of chronic aluminum exposure in mice. Fundam Appl Toxicol 1987;8:346–57.
[29] Donald JM, Golub MS, Gershwin ME, Keen CL. Neurobehavioral effects in offspring of mice given excess aluminum in diet during gestation and lactation. Neurotoxicol Teratol 1989;11:345–51.
[30] Golub MS, Keen CL, Gershwin ME. Neurodevelopmental effect of aluminum in mice: fostering studies. Neurotoxicol Teratol 1992;14:177–82.
[31] Golub MS, Han B, Keen CL, Gershwin ME, Tarara RP. Behavioral performance of Swiss Webster mice exposed to excess dietary aluminum during development or during development and as adults. Toxicol Appl Pharmacol 1995;133:64–72.
[32] Golub MS, Germann SL. Long-term consequences of developmental exposure to aluminum in a suboptimal diet for growth and behavior of Swiss Webster mice. Neurotoxicol Teratol 2001;23:365–72.
[33] Stauber JL, Florence TM, Davies CM, Adams MS, Buchanan SJ. Bioavailability of Al in alum-treated drinking water. J Am Water Works Assoc 1999;91:84–93.
[34] Schonholzer KW, Sutton RA, Walker VR, Sossi V, Schulzer M, Orvig C, et al. Intestinal absorption of trace amounts of aluminium in rats studied with 26 aluminium and accelerator mass spectrometry. Clin Sci (Lond) 1997;92:379–83.
[35] Taimei Chemicals Co., Ltd. Aluminium sulfate, product introduction. Available at: http://www.taimei-chem.co.jp/product/01.html [accessed 16.04.10].
[36] Donaldson L. The manufacture of aluminium sulfate. New Zealand Institute of Chemistry Website. Available at: http://nzic.org.nz/ChemProcesses/production/1F.pdf [accessed 16.04.10].
[37] OECD (Organisation for Economic Co-operation and Development). Two-generation reproduction toxicity study (Test No. 416, Adopted on January 22, 2001). OECD guidelines for testing of chemicals; 2001.
[38] MHW (Ministry of Health and Welfare, Japan). The guidelines for designation of food additives, and for revision of standards for use of food additives, Notification by director of Environmental Health Bureau, MHW (Eikahatsu No. 29), dated March 22, 1996.
[39] ME, METI, MHLW (Ministry of the Environment, Ministry of Economy, Trade and Industry, Ministry of Health, Labour and Welfare, Japan). Standard concerning testing laboratories implementing tests for new chemical substances etc., Joint notification by director generals of Environmental Policy Bureau, ME (Kanpokihatsu No. 031121004) and Manufacturing Industries Bureau, METI (Seikyokuhatsu No. 3), dated November 17, 2003 and by director general of Pharmaceutical and Food Safety Bureau, MHLW (Yakusyokuhatsu No. 1121003), dated November 21, 2003.
[40] ME, METI, MHLW (Ministry of the Environment, Ministry of Economy, Trade and Industry, Ministry of Health, Labour and Welfare, Japan). Partial amendment to "Standard concerning testing laboratories implementing tests for new chemical substances etc.", Joint notification by director generals of Environmental Policy Bureau, ME (Kanpokihatsu No. 080704001) and Manufacturing Industries Bureau, METI (Seikyokuhatsu No. 2), dated June 30, 2008 and by director general of Pharmaceutical and Food Safety Bureau, MHLW (Yakusyokuhatsu No. 0704001), dated July 4, 2008.
[41] Japanese animal welfare law "Act on Welfare and Management of Animals". Act No. 105 of October 1, 1973, as amended up to Act No. 68 of June 22, 2005.
[42] Act on Welfare and Management of Animals, Act No. 105 of October 1, 1973, as amended up to Act No. 68 of June 22, 2005.
[43] ME (Ministry of the Environment, Japan). Standards Relating to the Care, Management of Laboratory Animals and Relief of Pain. Announcement No. 88 of April 28, 2006.
[44] MHLW (Ministry of Health, Labour and Welfare, Japan). Fundamental Guidelines for Proper Conduct of Animal Experiment and Related Activities in the Testing Facility under the Jurisdiction of the Ministry of Health, Labour and Welfare. Notification by director of Health Sciences Division, Minister's Secretariat, MHLW (Kahatsu No. 0601005), dated June 1, 2006.
[45] Biel W. Early age differences in maze performance in the albino rats. J Genet Psychol 1940;56:439–45.
[46] Campbell MA, Golub MS, Iyer P, Kaufman FL, Li LH, Moran Messen F, et al. Reduced water intake: implications for rodent developmental and reproductive toxicity studies. Birth Defects Res B Dev Reprod Toxicol 2009;86:157–75.
[47] Kamboj VP, Kar AB. Antitesticular effect of metallic and rare earth salts. J Reprod Fertil 1964;7:21–8.
[48] Jouhanneau P, Raisbeck GM, Yiou F, Lacour B, Banide H, Drueke TB. Gastrointestinal absorption, tissue retention, and urinary excretion of dietary aluminum in rats determined by using 26Al. Clin Chem 1997;43:1023–8.
[49] Zafar TA, Weaver CM, Martin BR, Flarend R, Elmore D. Aluminum (26Al) metabolism in rats. Proc Soc Exp Biol Med 1997;216:81–5.
[50] Krasovskii GN, Vasukovich LY, Chariev OG. Experimental study of biological effects of leads and aluminum following oral administration. Environ Health Perspect 1979;30:47–51.
[51] ATSDR (Agency for Toxic Substance and Disease Registry). Toxicological profile for aluminum. Atlanta, Georgia: ATSDR, U.S. Department of Health and Human Services; 2008.
[52] Hicks JS, Hackett DS, Sprague GL. Toxicity and aluminium concentration in bone following dietary administration of two sodium aluminium phosphate formulations in rats. Food Chem Toxicol 1987;25:533–8.

[53] Katz AC, Frank DW, Sauerhoff MW, Zwicker GM, Freudenthal RI. A 6-month dietary toxicity study of acidic sodium aluminium phosphate in beagle dogs. Food Chem Toxicol 1984;22:7–9.
[54] Holson JF, Nemec MD, Stump DG, Kaufman LF, Lindström P, Varsho BJ. Significance, reliability, and interpretation of developmental and reproductive toxicity study findings. In: Hood RD, editor. Developmental and reproductive toxicology—a practical approach. 2nd ed. Florida: CRC Press, Taylor & Fransis Group; 2006. p. 329–424.
[55] Kennedy GC, Mitra J. Body weight and food intake as initiating factors for puberty in the rat. J Physiol 1963;166:408–18.
[56] Alleva E, Rankin J, Santucci D. Neurobehavioral alteration in rodents following developmental exposure to aluminum. Toxicol Ind Health 1998;14:209–21.
[57] Golub MS, Domingo JL. What we know and what we need to know about developmental aluminum toxicity. J Toxicol Environ Health 1996;48:585–97.
[58] Muller G, Bernuzzi V, Desor D, Hutin MF, Burnel D, Lehr PR. Developmental alterations in offspring of female rats orally intoxicated by aluminum lactate at different gestation periods. Teratology 1990;42:253–61.

WATER RESEARCH 45 (2011) 1720–1728

Available at www.sciencedirect.com

ScienceDirect

journal homepage: www.elsevier.com/locate/watres

Modeling high adsorption capacity and kinetics of organic macromolecules on super-powdered activated carbon

Yoshihiko Matsui, Naoya Ando, Tomoaki Yoshida, Ryuji Kurotobi, Taku Matsushita, Koichi Ohno*

Graduate School of Engineering, Hokkaido University, N13W8, Sapporo 060-8628, Japan

ARTICLE INFO

Article history:
Received 3 March 2010
Received in revised form
15 November 2010
Accepted 15 November 2010
Available online 24 November 2010

Keywords:
Diffusion
Isotherm
Shell
Equilibrium
Homogeneous
surface diffusion
model (HSDM)

ABSTRACT

The capacity to adsorb natural organic matter (NOM) and polystyrene sulfonates (PSSs) on small particle-size activated carbon (super-powdered activated carbon, SPAC) is higher than that on larger particle-size activated carbon (powdered-activated carbon, PAC). Increased adsorption capacity is likely attributable to the larger external surface area because the NOM and PSS molecules do not completely penetrate the adsorbent particle; they preferentially adsorb near the outer surface of the particle. In this study, we propose a new isotherm equation, the Shell Adsorption Model (SAM), to explain the higher adsorption capacity on smaller adsorbent particles and to describe quantitatively adsorption isotherms of activated carbons of different particle sizes: PAC and SPAC. The SAM was verified with the experimental data of PSS adsorption kinetics as well as equilibrium. SAM successfully characterized PSS adsorption isotherm data for SPACs and PAC simultaneously with the same model parameters. When SAM was incorporated into an adsorption kinetic model, kinetic decay curves for PSSs adsorbing onto activated carbons of different particle sizes could be simultaneously described with a single kinetics parameter value. On the other hand, when SAM was not incorporated into such an adsorption kinetic model and instead isotherms were described by the Freundlich model, the kinetic decay curves were not well described. The success of the SAM further supports the adsorption mechanism of PSSs preferentially adsorbing near the outer surface of activated carbon particles.

1. Introduction

It has been thought that adsorption capacity of activated carbon does not depend on particle size because adsorption occurs in internal pores of activated carbon particles (Letterman et al., 1974; Najm et al., 1990; Peel and Benedek, 1980a and Leenheer, 2007); however, the effect of adsorbent particle size on adsorption capacity has not been examined sufficiently. With decreasing activated carbon particle size, the capacity to adsorb natural organic matter (NOM) has been reported both to not change (Randtke and Snoeyink, 1983) and to increase (Weber et al., 1983). Possible reasons for these contradictory results have been discussed, but a clear mechanism with supporting experimental evidence has not yet been presented.

Recently, very fine (median particle diameters of 0.7 μm) activated carbon particles (super-powdered activated carbon, SPAC) became available through advances in pulverization technology (Matsui et al., 2004, 2005, 2007, 2009a). Thus, it has become possible to reduce adsorbent particle diameter to the submicron range, which is ten times as small as the size of powdered-activated carbon (PAC). SPAC adsorbs NOM

* *Corresponding author.* Tel./fax: +81 11 706 7280.
E-mail address: matsui@eng.hokudai.ac.jp (Y. Matsui).
0043-1354/$ – see front matter © 2010 Elsevier Ltd. All rights reserved.
doi:10.1016/j.watres.2010.11.020

efficiently because of its high adsorption capacity as well as its kinetic properties. The high adsorption capacity of SPAC raises the issue of adsorption capacity dependence on adsorbent particle size. In the early stages of SPAC research, increased capacity for NOM adsorption on SPAC was thought to be attributable to the mesopore volume increase caused by the fracture of ink-bottle pore structures during pulverization (Matsui et al., 2004). However, it later became apparent that structural changes in pore size distribution attributable to pulverization were not large, and the capacity increase for NOM adsorption could not be explained adequately by an increase in mesopore volume. Instead, it has been proposed that the capacity increase for NOM adsorption on SPAC is due to adsorbate not penetrating completely into the adsorbent particle and preferentially adsorbing in the particle outer region close to the surface of the particle; we also proposed a conceptualization of this concept (Ando et al., 2010).

The objective of our current research is to verify and confirm this conceptualization through model analysis. To do so, we have developed adsorption isotherm and kinetic models based on the shell adsorption mechanism, and verified our findings with experimental data by using polystyrene sulfonates (PSSs) as model substances (Karanfil et al., 1996a,b; Li et al., 2003a,b; and Ando et al., 2010).

2. Materials and methods

2.1. Activated carbons

Commercially available PAC (Taikou-W, Futamura Chemical Industries Co., Ltd., Gifu, Japan) was used as received (PAC-T) or pulverized in a bead mill (Metawater Co., Ltd., Tokyo, Japan) to achieve four degrees of pulverization; we designated these super-powdered activated carbons as SPACa-T, SPACb-T, SPACc-T, and SPACd-T, in increasing order of particle size. The pore size distributions and the scanning electron micrographs of SPACa-T and PAC-T are presented elsewhere (Ando et al., 2010). Slurries of each activated carbon were prepared in pure water and stored at 4 °C and used after dilution and placement under vacuum. Particle size distributions of the five activated carbons were determined by using a laser-light scattering instrument (LA-700, Horiba, Ltd., Kyoto, Japan).

2.2. Water samples

PSSs with various molecular weights (MWs) were selected as model substances instead of NOM because PSSs are chemically homogeneous compounds with known MWs and narrow MW ranges, while NOM is a complex mixture of compounds with unknown composition. Thus, our selection of PSSs makes model analysis of adsorption equilibrium and kinetics clear and unambiguous. We refer to our first PSS formulation as PSS-4600 (Polysciences, Inc., Warrington PA, USA), with a weight-average MW (Mw) of 5180 Da and a number-average MW (Mn) of 4600 Da. Our second PSS formulation, referred to as PSS-1800 (Polysciences, Inc.), had an Mw of 1430 Da and an Mn of 1200 Da. Our final PSS formulation, referred to as PSS-1000 (Polymer Standard Service GmbH., Mainz, Germany), had an Mw of 1100 Da and an Mw/Mn of <1.2.

We dissolved the PSSs in ultrapure water after the addition of inorganic ions to adjust the ionic strength, and we adjusted the constituent inorganic ions and their concentrations to match those of natural water and the PSS waters used in previous experiments (Table 1S in the supplementary information, Matsui et al., 2004; Ando et al., 2010). All water samples were adjusted to pH 7.0 ± 0.1 by the addition of HCl or NaOH, as required; they were then filtered through 0.2-μm membrane filters (DISMIC-25HP, Toyo Roshi Kaisha, Ltd., Tokyo) before use in experiments. We determined PSS concentrations by UV absorption at a wavelength of 262 nm (UV-1700, Shimadzu Co., Kyoto, Japan).

2.3. Batch adsorption tests

We conducted PSS-1800 and PSS-1000 adsorption equilibrium tests with all five activated carbons, but we conducted PSS-4600 adsorption equilibrium tests only with SPACa-T, SPACd-T, and PAC-T. The experimental procedure, described in detail elsewhere (Ando et al., 2010), briefly is as follows. SPAC and PAC slurries were diluted, placed under vacuum, and added to 300-mL solutions containing adsorbate with mixing (Table 2S in the supplementary information). Aliquots (100 mL) were transferred from the 300-mL solutions to 125-mL vials, which were agitated on a shaker for 3 weeks at a constant temperature of 20 °C. Control tests were also conducted that did not contain carbon to confirm that concentration changes during long-term mixing were negligible. After filtering the water samples through a 0.2-μm membrane filter, we measured the liquid-phase adsorbate concentrations.

We investigated adsorption kinetics of SPACa-T, SPACd-T, and PAC-T by means of batch tests with efficient mixing. Sample water (3 L) containing PSSs was placed in a beaker, and an aliquot (50 mL) was withdrawn from the beaker to determine the initial PSS concentration. After the addition of a specified amount of an activated carbon suspension (Table 3S in the supplementary information), aliquots (50 mL) were withdrawn at intervals and filtered immediately through a 0.2-μm membrane filter for determination of PSS concentration.

3. Results and discussion

3.1. Shell adsorption model

Clearly adsorption capacity for PSS-4600, PSS-1800, and PSS-1000 on activated carbon (SPACa-T, SPACb-T, SPACc-T, SPACd-T, and PAC-T) increased with decreasing adsorbent particle size (Fig. 1 and Fig. 1S in the supplementary information). Adsorption sharply increased with increasing equilibrium concentration close to the initial concentration, in particular for PSS-1000. This could be due to the heterogeneity of PSS compounds (Karanfil et al., 1996a; Matsui et al., 1998), despite our assumption of homogeneity for the PSS compounds because of their small-MW ranges. Therefore, the data points for concentrations close to the initial concentration, indicated by red color in Fig. 1, were omitted from our mathematical analysis. Adsorption capacity for all three PSS formulations, as represented by q_{50}, increased with decreasing adsorbent particle size (Fig. 2). PSS adsorption

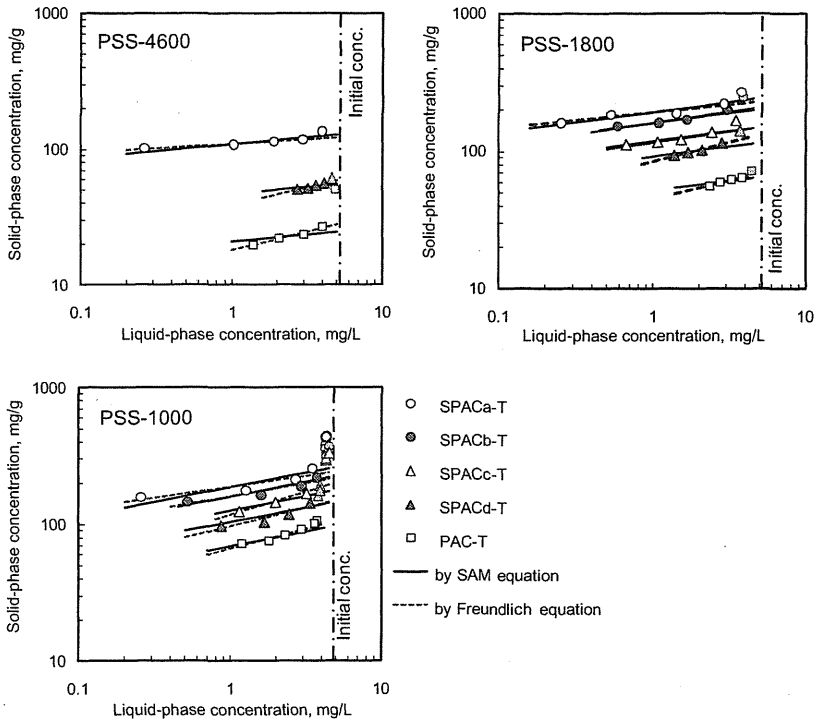

Fig. 1 – Adsorption isotherms of PSS-4600 (upper left panel), PSS-1800 (upper right panel), and PSS-1000 (lower panel). Lines are SAM and Freundlich fits to data (plots close to the initial concentration are red-colored) (For interpretation of the references to colour in this figure legend, the reader is referred to the web version of this article).

capacity on SPACa-T (d_{50} = 0.7 μm), which had the smallest particle size, was highest, followed by SPACb-T (d_{50} = 1.1 μm), SPACc-T (1.9 μm), SPACd-T (3.0 μm), and PAC-T (11.8 μm), in increasing order of particle size: d_{50} is a volumetric median particle diameter, and q_{50} is defined as the amount adsorbed on activated carbon in equilibrium with 2.5 mg/L liquid-phase concentration equal to half the initial concentration (5 mg/L) in the adsorption experiment. Ando et al. (2010) hypothesize that the increase in adsorption capacity with decreasing adsorbent particle size is attributable to molecules adsorbing principally in the exterior region close to the external particle surface. The specific external surface area (surface area per unit mass) available for adsorption would be greater for smaller adsorbent particles, and hence adsorption capacity could be larger on SPAC, which had a much smaller particle size than PAC.

In adsorption isotherm model equations, such as the Freundlich equation, amount adsorbed is expressed as mass of adsorbate per unit mass of adsorbent (e.g., Sontheimer et al., 1988). This relationship implicitly assumes that adsorption surface area is proportional to mass of adsorbent and that adsorption capacity is independent of adsorbent particle size. In a previous study (Karanfil et al., 1996a), the Freundlich equation has been employed successfully to describe adsorption isotherms of PSSs, but the effect of adsorbent size was not studied. In our current research, we

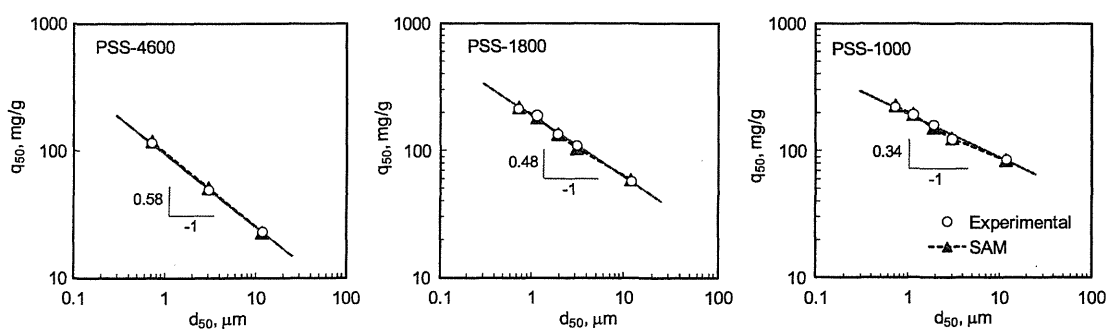

Fig. 2 – PSS adsorption capacities represented by q_{50} against volumetric median diameters of adsorbents. q_{50} is defined as the amount adsorbed on activated carbon in equilibrium with 2.5 mg/L liquid-phase concentration equal to half of initial concentration (5 mg/L) in the adsorption experiment.

have modified the Freundlich equation, as per Eq. (1), in order to describe adsorption capacity dependence on adsorbent particle size, as follows:

$$q_E = KC_E^{1/n} \quad (1)$$

where q_E is the amount adsorbed in solid-phase in equilibrium with liquid-phase concentration (mg/g), C_E is the liquid-phase concentration (mg/L), K is the Freundlich adsorption capacity parameter (mg/g)/(mg/L)$^{1/n}$, and n is the Freundlich exponent.

Beginning with the Freundlich approach, we have modeled the mechanism of Ando et al. (2010) such that the adsorption capacity parameter K is assumed to decrease with increasing distance from the adsorbent particle surface. Using radial coordinates, the Freundlich adsorption capacity parameter is a function of radial distance and particle radius; adsorption capacity of an adsorbent with radius R at radial distance r is then given by Eq. (2), as follows:

$$q_S(r,R) = K_S(r,R)C_E^{1/n} \quad (2)$$

where r is the radial distance from the center of a PAC particle (μm), R is the adsorbent particle radius (μm), $q_S(r, R)$ is the local solid-phase concentration (mg/g) at radial distance r in an adsorbent with radius R, and $K_S(r, R)$ is the radially changing Freundlich adsorption capacity parameter (mg/g)/(mg/L)$^{1/n}$ as a function of radial distance r and adsorbent radius R. Spherical particles were assumed for the PAC and the SPACs, which is the conventional practice for adsorption kinetic models (e.g., Sontheimer et al., 1988).

Therefore, adsorption capacity of an adsorbent with particle radius R in equilibrium with liquid-phase concentration C_E is given by Eq. (3), as shown below:

$$\int_0^R q_S(r,R)\frac{3r^2}{R^3}dr = C_E^{1/n}\frac{3}{R^3}\int_0^R K_S(r,R)r^2dr \quad (3)$$

Accordingly, when the adsorbent size is not uniform, the overall adsorption capacity of the adsorbent is given by Eq. (4), as follows

$$q_E = C_E^{1/n}\frac{3}{R^3}\int_0^\infty\left[\int_0^R K_S(r,R)r^2dr\right]f_R(R)dR \quad (4)$$

where q_E is the overall adsorption capacity of adsorbent (mg/g), and $f_R(R)$ is the normalized particle size distribution function of adsorbent (μm^{-1}).

As a model for $K_S(r, R)$, we adopted Eq. (5), in which adsorption capacity linearly decreases with distance from the external surface to a depth, δ, but thereafter some of the adsorption capacity remains at a level, p, inward from that depth, as depicted in Fig. 3:

$$K_S(r,R) = K_0\left[\max\left(\frac{r-R+\delta}{\delta},0\right)(1-p)+p\right] \quad (5)$$

where K_0 is the Freundlich parameter of adsorption at the external particle surface (K_0 means solid-phase concentration at $r = R$ at unity equilibrium concentration, (mg/g)/(mg/L)$^{1/n}$), δ is the penetration depth (or thickness of the penetration shell, μm), and p is a dimensionless parameter that defines availability of internal porous structures for adsorption.

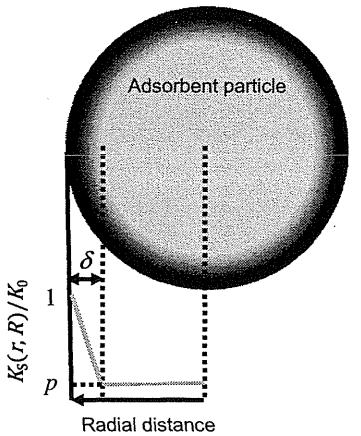

Fig. 3 – Schematic diagram of SAM. Molecules adsorb principally in the exterior region (black region in the figure) close to the particle surface, but to some extent do diffuse into the inner region (light gray region in the figure) of an adsorbent particle. $K_S(r, R)/K_0$, normalized adsorption capacity relative to the adsorption capacity at the external surface linearly decreases with distance from the external surface to a depth δ, (from black to dark gray region) in the figure and thereafter (light gray region) it remains constant as p.

Eq. (5) evolved from the following reasoning: If adsorption occurs only at external particle surface, then adsorption capacity increase is inversely proportional to adsorbent particle size (slope of log q_{50} vs. log $d_{50} = -1$). However, slopes for data points (Fig. 2) range only from −0.34 to −0.58 (less steep than −1), thereby indicating that some of the interior region of the adsorbent particles is available for adsorption. Some adsorbate molecules probably diffuse into and adsorb onto the interior region, while other molecules adsorb onto the exterior region close to the particle outer surface (shell region).

The final form of the isotherm equation, referred to hereinafter as the Shell Adsorption Model (SAM) equation, is expressed as Eq. (6)

$$q_E = C_E^{1/n}\frac{3K_0}{R^3}\int_0^\infty\left\{\int_0^R\left[\max\left(\frac{r-R+\delta}{\delta},0\right)(1-p)+p\right]r^2dr\right\}f_R(R)dR \quad (6)$$

We have applied this SAM equation to describe isotherm data shown in Fig. 1; in doing so, we sought a single set of isotherm parameter values for K_0, n, δ, and p in order to obtain the best model fit to data for PSS adsorption isotherms of SPACa-T, SPACb-T, SPACc-T, SPACd-T, and PAC-T. SAM satisfactorily described the experimental data, as shown in Figs. 1 and 2. Our SAM equation is a modified version of the Freundlich equation that is extended so that the slope in the log–log plot of solid-phase concentration vs. liquid-phase concentration is identical for each of the activated carbon preparations. However, experimentally measured slopes for SPACa-T and SPACb-T were actually slightly less steep than those for SPACd-T and PAC-T when applying the Freundlich

equation to data for each activated carbon (see dashed lines in Fig. 1 and Table 1). Because the change in slope after pulverization was not very marked, however, we feel that the SAM approach was successful in providing a first estimate of the dependence of adsorption capacity on particle size.

3.2. *Adsorption kinetics in the shell adsorption model*

We analyzed adsorption kinetics data to determine whether incorporation of the SAM equation into an adsorption kinetic model adequately describes the kinetics data. In combining the kinetic model with SAM, we used the pore diffusion model (PDM, e.g., Sontheimer et al., 1988). Although the homogeneous surface diffusion model (HSDM) is more widely used than PDM (Sontheimer et al., 1988), we felt that it could not be applied because it assumes homogeneity inside activated carbon particles. Such homogeneity implies that adsorbed molecules have migrated into adsorbent particles by Fick's first law of diffusion according to a local solid-phase concentration gradient, and that adsorbate molecules are ultimately distributed evenly along an adsorbent gradient such that local solid-phase concentrations become equal. Such a scenario is inconsistent with SAM. Therefore, instead of HSDM, we used PDM in which migration of molecules in the liquid-filled pores contributes to transport of adsorbates into particles, while local solid-phase and liquid-phase concentrations in pores remain at equilibrium during the entire period of adsorption (instantaneous adsorption). At an adsorption equilibrium condition in PDM, local liquid-phase concentrations become equal, while local solid-phase concentrations do not necessarily become equal; that condition does not violate SAM. Local adsorption equilibrium is expressed by Eq. (7), as follows:

$$c(t,r,R) = \left(\frac{q(t,r,R)}{K_S(r,R)}\right)^n \tag{7}$$

where t is adsorption time in the batch system (s); $c(t, r, R)$ is the liquid-phase concentration in an adsorbent particle having radius R at radial distance r and time t (mg/L); and $q(t, r, R)$ is the solid-phase concentration in an adsorbent particle having radius R at radial distance r and time t (mg/g).

Diffusion of adsorbate molecules in an adsorbent particle is expressed by Eq. (8), as follows

$$\frac{\partial q(t,r,R)}{\partial t} = \frac{D_P}{\rho}\frac{1}{r^2}\frac{\partial}{\partial r}\left(r^2\frac{\partial c(t,r,R)}{\partial r}\right) \tag{8}$$

where D_P is the pore diffusion coefficient (cm^2/s); and ρ is adsorbent particle density (g/L).

Table 1 – Equilibrium and kinetic parameters and E_{NS} values.

PSS-4600	Simulation 1	Simulation 2	Simulation 3
Adsorption equilibrium	SAM $K_0 = 1.8 \times 10^2$ (mg/g)/(mg/L)$^{1/n}$ $1/n = 0.10$ $\delta = 0.22$ μm $p = 0.038$	Freundlich K (SPACa-T) = 110 (mg/g)/(mg/L)$^{1/n}$ 1/n (SPACa-T) = 0.064 K (SPACd-T) = 39 (mg/g)/(mg/L)$^{1/n}$ 1/n (SPACd-T) = 0.26 K (PAC-T) = 18 (mg/g)/(mg/L)$^{1/n}$ 1/n (PAC-T) = 0.27	
Adsorption kinetics	PDM $D_P = 2.9 \times 10^{-10}$ cm^2/s	HSDM $D_S = 3.3 \times 10^{-13}$ cm^2/s	PDM $D_P = 1.7 \times 10^{-9}$ cm^2/s
E_{NS}	0.25	−2.1	−0.49
PSS-1800	**Simulation 1**	**Simulation 2**	**Simulation 3**
Adsorption equilibrium	SAM $K_0 = 3.2 \times 10^2$ (mg/g)/(mg/L)$^{1/n}$ $1/n = 0.15$ $\delta = 0.20$ μm $p = 0.095$	Freundlich K (SPACa-T) = 190 (mg/g)/(mg/L)$^{1/n}$ 1/n (SPACa-T) = 0.11 K (SPACd-T) = 85 (mg/g)/(mg/L)$^{1/n}$ 1/n (SPACd-T) = 0.28 K (PAC-T) = 45 (mg/g)/(mg/L)$^{1/n}$ 1/n (PAC-T) = 0.28	
Adsorption kinetics	PDM $D_P = 7.6 \times 10^{-10}$ cm^2/s	HSDM $D_S = 2.1 \times 10^{-13}$ cm^2/s	PDM $D_P = 3.2 \times 10^{-9}$ cm^2/s
E_{NS}	0.85	0.11	0.71
PSS-1000	**Simulation 1**	**Simulation 2**	**Simulation 3**
Adsorption equilibrium	SAM $K_0 = 2.8 \times 10^2$ (mg/g)/(mg/L)$^{1/n}$ $1/n = 0.21$ $\delta = 0.21$ μm $p = 0.18$	Freundlich K (SPACa-T) = 190 (mg/g)/(mg/L)$^{1/n}$ 1/n (SPACa-T) = 0.16 K (SPACd-T) = 97 (mg/g)/(mg/L)$^{1/n}$ 1/n (SPACd-T) = 0.27 K (PAC-T) = 67 (mg/g)/(mg/L)$^{1/n}$ 1/n (PAC-T) = 0.28	
Adsorption kinetics	PDM $D_P = 11.0 \times 10^{-10}$ cm^2/s	HSDM $D_S = 1.5 \times 10^{-13}$ cm^2/s	PDM $D_P = 3.3 \times 10^{-9}$ cm2/s
E_{NS}	0.40	−0.84	0.083

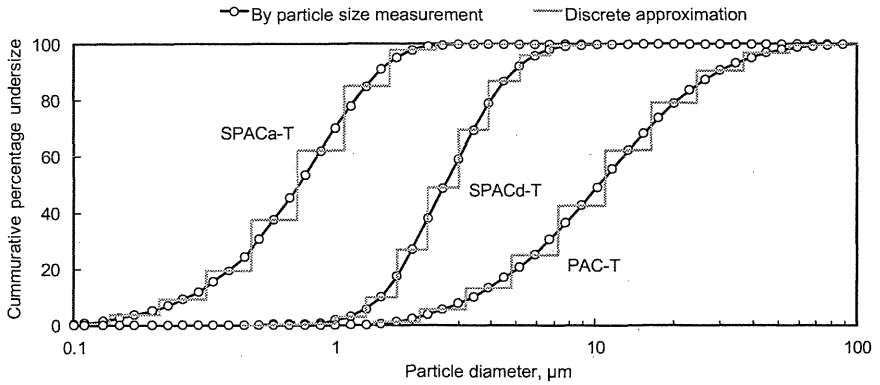

Fig. 4 – Particle size distributions of SPACa-T, SPACd-T, and PAC-T.

External film balance is described by equating mass balance and mass transfer from the external particle surface to inside the particle, as shown in Eq. (9):

$$\frac{d}{dt}\left[\int_0^R r^2 q(t,r,R)dr\right]\frac{1}{R^2} = \frac{k_f}{\rho}[C(t) - c(t,R,R)] \tag{9}$$

where k_f is the liquid film mass transfer coefficient (cm/s), ρ is the adsorbent particle density (g/L), and C(t) is the adsorbate concentration in the bulk water phase as a function of time, t (mg/L).

When considering adsorbent particle size distribution (Matsui et al., 2003), the mass balance equation for an adsorbate in a batch reactor is given in Eq. (10), as follows:

$$\frac{dC(t)}{dt} = -\frac{3C_C k_f}{\rho}\int_0^\infty \frac{f_R(R)}{R}[C(t) - c(t,R,R)]dR \tag{10}$$

We approximated particle size distribution of adsorbent by a discrete density function consisting of M size classes, where M is 13, as shown in Fig. 4. We converted the set of model Eqs (5) and (7)–(10) for adsorption in a batch reactor into a set of ordinary differential equations with respect to time, t, using the method of orthogonal collocation. We took many collocation points in an attempt to describe precisely the change of solid-phase concentration in the vicinity of the particle surface (shell region in Fig. 3). When the number of collocation points was 40, the shell region of a PAC particle 11.8 μm in diameter was divided by 6 in the radial direction and that of a SPAC particle 0.7 μm in diameter was divided by 30. Resultant equations were solved as a system of ordinary differential equations by Gear's stiff method in the IMSL® Math Library, after deriving the analytical Jacobian of the equations (Matsui et al., 2009b). Mass transfer resistance across the liquid film external to the adsorbent particle surfaces was substantially neglected because it cannot be the rate-determining step in well-mixed reactors (Sontheimer et al., 1988). In model simulations, the liquid film mass transfer coefficient (k_f) was set to 10 cm/s, at which value liquid film mass transfer did not control adsorbate uptake to adsorbent, because any values larger than 10 cm/s yielded the same simulation results for concentration decay curves. Finally, a single value of pore diffusion coefficient D_p, the remaining unknown model parameter in PDM, was sought by using quasi-Newton method in the IMSL® Math Library and then the D_p value was determined that produced best-fits to the experimental data for SPACa-T, SPACd-T, and PAC-T under the minimum error criterion [maximizing the E_{NS} value defined by Eq. (11)], as follows:

$$E_{NS} = 1 - \frac{\sum_{j=1}^{N}(C_{obs,j} - C_{cal,j})^2}{\sum_{j=1}^{N}(C_{obs,j} - C_{ave})^2} \tag{11}$$

where $C_{obs,j}$ and $C_{cal,j}$ are the observed and calculated concentrations (mg/L) of adsorbate, respectively; C_{ave} is the average concentration of adsorbate (mg/L); and N is the

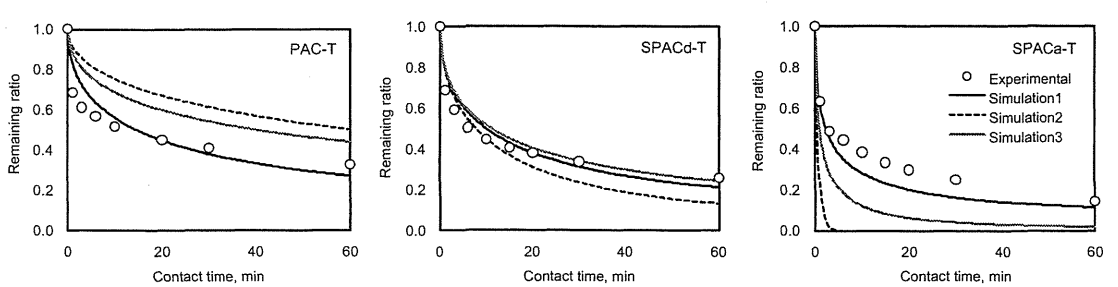

Fig. 5 – PSS-4600 adsorption kinetics data and curves fitted with three models (Initial PSS-4600 concentration was 5 mg/L. PAC-T, SPACd-T, and SPACa-T doses were 500, 200, and 100 mg/L, respectively).

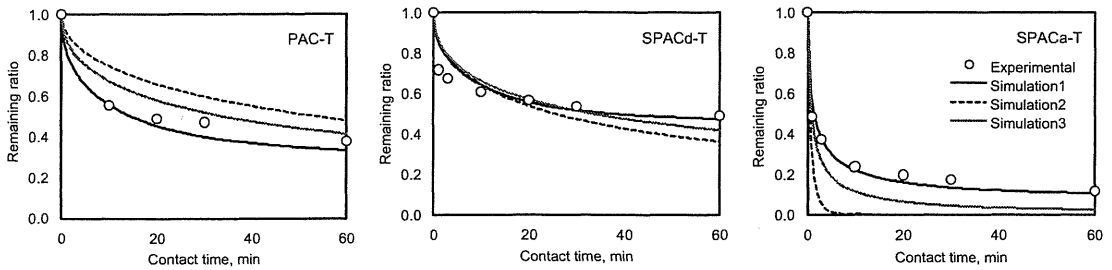

Fig. 6 – PSS-1800 adsorption kinetics data and curves fitted with models (Initial PSS-1800 concentration was 5 mg/L. PAC-T, SPACd-T, and SPACa-T doses were 200, 50, and 50 mg/L, respectively).

number of data points. E_{NS} values vary between $-\infty$ and 1; a value of 1.0 indicates a perfect fit.

As a comparison to the SAM + PDM model (to be called Simulation 1 hereinafter), we used the Freundlich model + HSDM (Simulation 2) and the Freundlich model + PDM (Simulation 3). In these cases, the Freundlich model parameters were individually determined for each activated carbon sample (SPACa-T, SPACd-T, and PAC-T) from the corresponding set of isotherm data. Then, from adsorption kinetics data, a single value for the surface diffusion coefficient D_S was sought under the minimum error criterion to simulate experimental data sets for SPACa-T, SPACd-T, and PAC-T (Simulation 2) [Matsui et al., 2003]. A single value of the pore diffusion coefficient D_P was sought in Simulation 3. Isotherm model parameter values determined from experimental data of Fig. 1 and the D_P and D_S values searched are summarized in Table 1.

All PSS kinetics curves featured a sharp concentration drop in the first few minutes, followed by a subsequent slower decrease (Figs. 5–7). Experimental data for all PSS kinetics are the best described by the SAM + PDM model, into which a single D_P value was inserted. E_{NS} value for PSS-1000, for example, was 0.40 (Table 1). Freundlich model + HSDM simulations carried out with one D_S value (Simulation 2) did not fit experimental data for activated carbons of small and large size: E_{NS} value was −0.84. Freundlich model + HSDM simulations underestimate solute uptake rate into large particle-size adsorbent (PAC-T) and overestimate solute uptake rate into small particle size adsorbent (SPACa-T). Simulation 3, carried out with one D_P value, also did not adequately describe PSS adsorption kinetics for PAC-T and SPACa-T (E_{NS} value was 0.083). Simulation 1 was also reasonable in terms of diffusivity and MW: the smallest molecule, PSS-1000, had the highest diffusivity, followed by PSS-1800; and the largest molecule, PSS-4600, had the lowest diffusivity (the D_P values of PSS-4600, -1800, and -1000 were 2.9×10^{-10}, 7.6×10^{-10}, and 11.0×10^{-10} cm^2/s, respectively; see Table 1). Such a relationship between diffusivity and MW was not observed in Simulations 2 and 3.

In our simulations using the Freundlich model + HSDM and the Freundlich model + PDM, we employed six adjustable parameters (2 model parameters times 3 carbons) to describe adsorption isotherms for the three activated carbon preparations: that is, we determined distinct K and $1/n$ values for SPACa-T, SPACd-T, and PAC-T by linear regression. On the other hand, SAM has four adjustable model parameters for all the three carbons. When considering only the number of adjustable model parameters, the SAM + PDM model should have two less degrees of freedom in describing a variety of adsorption kinetics than the Freundlich model + HSDM or the Freundlich model + PDM. Our results, however, show that SAM + PDM was more accurate in describing adsorption kinetics than the Freundlich model + HSDM or the Freundlich model + PDM. The Freundlich model + HSDM or Freundlich model + PDM simulations underestimate solute uptake rate into the large particle-size adsorbent (PAC-T). Implementation of SAM contributed to the solving this underestimation problem by enhancing adsorbate uptake rate. We attribute this enhancement to the fact that most adsorbate molecules do not diffuse into the inner region of adsorbent particles before reaching adsorption equilibrium. Thus, most of the adsorption process is complete close to the exterior particle surface. Therefore, the superiority of the SAM + PDM model is attributable to the shell adsorption mechanism, and our finding of a better data fit to the SAM + PDM model offers further evidence that PSS molecules adsorb mostly near the adsorbent

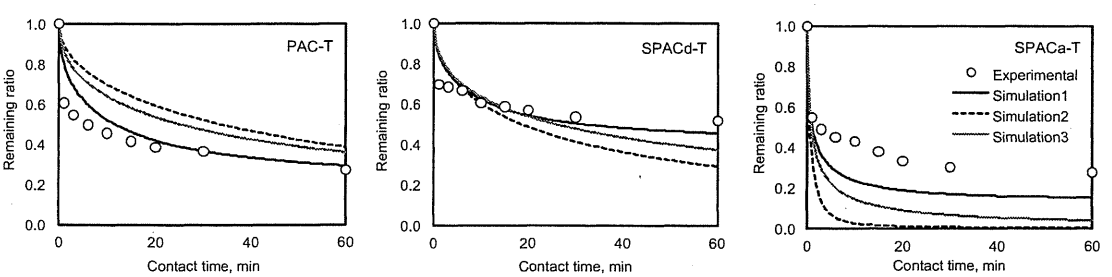

Fig. 7 – PSS-1000 adsorption kinetics data and curves fitted with models (Initial PSS-1000 concentration was 5 mg/L. PAC-T, SPACd-T, and SPACa-T doses were 200, 50, and 50 mg/L, respectively).

particle surface. We believe that the shell adsorption concept provides the best mechanism for describing adsorption kinetics on activated carbons with various particle sizes.

While the discrepancies between the experimental kinetics data and data obtained from Simulation 1 (SAM + PDM) could be partly due to experimental errors, we note some trends. For most experimental data of PAC-T and SPACd-T, concentrations drop rapidly as adsorption begins. However, initial adsorptions were slower in the simulations. On the other hand, the concentrations of SPACa-T for PSS-4600 and -1000 declined faster in the simulations than we observed in our experiments. This pattern of change could be related to local slow diffusion from macropore to micropore, which follows relatively rapid radial diffusion in macropore regions in the adsorbent (Sontheimer et al., 1988; Peel and Benedek, 1980a,b). Adsorption kinetics of a small-MW adsorbate, geosmin, which could adsorb on micropores of SPAC and PAC, is better described by a branched-pore kinetic model (BPKM), in which a slow diffusion mechanism is incorporated into HSDM (Matsui et al., 2009b). We have confirmed that PSS concentration decay curves are also better defined when a slow diffusion mechanism is incorporated into PDM, and the resulting simulation is more successful (data not shown). This improvement may be due to the number of adjustable model parameters for adsorption kinetics increasing from 1 to 3 with implementation of the slow diffusion mechanism.

Further research will be necessary to elucidate the slow diffusion mechanism for PSS adsorption. In this study, we have focused on the fact that application of the shell adsorption mechanism, whereby the compounds we studied adsorb mostly in the vicinity of external adsorbent particle surfaces, dramatically improves modeling of adsorption kinetics as well as isotherms. To enhance our understanding of the adsorption mechanism, we have modeled the adsorption of PSSs which are homogeneous compounds with a defined structure, but with a molecular size similar to that of NOM. In future work, adsorption behavior of NOM must be modeled in order to elucidate its adsorption capacity increase with decreasing adsorbent particle size. However, applying SAM to NOM may be difficult, as NOM is an extremely polydisperse mixture, with MWs ranging from hundreds to tens of thousands. Therefore, the parameter values of δ and p might vary for the various adsorbates with different properties (including MW) within each NOM solution.

The results of the current research may change the paradigm of rapid small-scale column tests (RSSCTs, Crittenden et al., 1986a,b). Our simulation by SAM-PDM implies that adsorption capacity is particle size dependent but that the intraparticle diffusion coefficient is not. The paradigm of SAM-PDM is opposite to that used to scale NOM adsorption in RSSCTs. RSSCTs for NOM adsorption implicitly assume the independence of adsorption capacity from carbon particle size and the proportional diffusivity (PD, the intraparticle diffusion coefficient linearly decreases with particle size). The RSSCT method is well supported by RSSCT data for NOM removal (e.g., Crittenden et al., 1991; Summers et al., 1995). One simple way to reconcile the SAM paradigm with the RSSCT is hypothesising that PAC adsorption capacity is dependent on carbon particle size but that GAC (granular activated carbon) adsorption capacity is not, because GAC has developed macropores that enable PSS and NOM molecules to penetrate inside of carbon particles and which then equalize carbon capacity regardless of carbon particle size (Ando et al., 2010). The diffusivity issue could be resolved if the SAM-PDM would better fit our experimental data when diffusivity was treated as variable rather than constant.

In addition to kinetics, adsorption capacity is a critical parameter that must be considered in the design of RSSCTs (Crittenden et al., 1986a; Sontheimer et al., 1988). Since RSSCTs are conducted on a sieved small-size fraction of crushed carbon particles instead of on the original as-received GAC, which is used in the full-scale adsorber, for proper design of RSSCTs it is essential to understand how not only the adsorption kinetics but also the adsorption capacity is affected by particle size. Actually, capacity increases with decreasing carbon particle size are reported for GACs (Randtke and Snoeyink, 1983; Weber et al., 1983). Moreover, the theoretical background is weak for the PD on which the design of RSSCTs relies. For synthetic organic chemicals (SOCs), on the other hand, isotherm capacities are not affected by carbon particle size (Letterman et al., 1974; Najm et al., 1990 and Leenheer, 2007). The independence of SOC adsorption capacity from carbon particle size is also held for SPAC and PAC (Matsui et al., 2004; Ando et al., 2010). For SOC removals, the RSSCT data well support the assumption of constant diffusivity (Crittenden et al., 1986a). We feel, therefore, that the method of RSSCT design for NOM adsorption could be improved through the study of how NOM adsorption capacity is affected by GAC particle size.

4. Conclusions

1) We have proposed a shell adsorption mechanism by which PSS molecules are principally adsorbed in the exterior (shell) region of activated carbon particles and adsorbed less in the interior region. The increasing adsorption capacity with decreasing particle size is explained by the increase in specific external surface area (surface area per unit mass) available for adsorption with decreasing adsorbent particle size. Therefore, the PSS adsorption capacity of SPAC was higher than that of PAC.
2) We have proposed a new isotherm equation (SAM), which incorporates the shell adsorption mechanism into the Freundlich model, and we have successfully described PSS adsorption isotherms for SPACs and PAC with the same model parameters.
3) PSS adsorption kinetics were described much better by SAM incorporated into PDM than by the conventional approaches of the Freundlich model + HSDM or the Freundlich model + PDM, which further supports our proposed shell adsorption mechanism.

Acknowledgments

This study was supported by a Grant-in-Aid for Scientific Research A (21246083) from the Ministry of Education, Science,

Sports, and Culture of the Government of Japan; by a research grant from the Ministry of Health, Labor, and Welfare; and by Metawater Co., Tokyo, Japan.

Appendix. Supplementary information

Additional details, including Tables 1S, 2S, and 3S and Figures 1S, are available in the online version at doi:10.1016/j.watres.2010.11.020.

REFERENCES

Ando, N., Matsui, Y., Kurotobi, Y., Nakano, Y., Matsushita, T., Ohno, K., 2010. Comparison of natural organic matter adsorption capacities of super-powdered activated carbon and powdered activated carbon. Water Res. 44 (14), 4127–4136.

Crittenden, J.C., Berrigan, J.K., Hand, D.W., 1986a. Design of rapid small-scale adsorption tests for a constant diffusivity. J. Water Pollut. Control Fed. 58 (4), 312–319.

Crittenden, J.C., Berrigan, J.K., Hand, D.W., Lykins, B., 1986b. Design of rapid small-scale adsorption tests for nonconstant diffusivity. J. Environ. Eng.–ASCE 113 (2), 243–259.

Crittenden, J.C., Reddy, P.S., Arora, H., Trynoski, J., Hand, D.W., Perram, D.L., Summers, R.S., 1991. Predicting GAC performance with rapid small-scale column tests. J. Am. Water Works Assoc. 83 (1), 77–87.

Karanfil, T., Kilduff, J.E., Schlautman, M.A., Weber Jr., W.J., 1996a. Adsorption of organic macromolecules by granular activated carbon. 1. Influence of molecular properties under anoxic solution conditions. Environ. Sci. Technol. 30 (7), 2187–2194.

Karanfil, T., Schlautman, M.A., Kilduff, J.E., Weber Jr., W.J., 1996b. Adsorption of organic macromolecules by granular activated carbon. 2. Influence of dissolved oxygen. Environ. Sci. Technol. 30 (7), 2195–2201.

Leenheer, J.A., 2007. Progression from model structures to molecular structures of natural organic matter components. Annals of Environ. Sci. 1, 57–68.

Letterman, R.D., Quon, J.E., Gemmell, R.S., 1974. Film transport coefficient in agitated suspensions of activated carbon. J. Water Pollut. Control Fed. 46 (11), 2536–2547.

Li, Q., Snoeyink, V.L., Mariãas, B.J., Campos, C., 2003a. Elucidating competitive adsorption mechanisms of atrazine and NOM using model compounds. Water Res. 37 (4), 773–784.

Li, Q., Snoeyink, V.L., Mariñas, B.J., Campos, C., 2003b. Three-component competitive adsorption model for flow-through PAC systems. 1. Model development and verification with a PAC/membrane system. Environ. Sci. Technol. 37 (13), 2997–3004.

Matsui, Y., Yuasa, A., Li, F., 1998. Overall adsorption isotherm of natural organic matter. J. Environ. Eng.–ASCE 124 (11), 1099–1107.

Matsui, Y., Fukuda, Y., Inoue, T., Matsushita, T., 2003. Effect of natural organic matter on powdered activated carbon adsorption of trace contaminants: characteristics and mechanism of competitive adsorption. Water Res. 37 (18), 4413–4424.

Matsui, Y., Fukuda, Y., Murase, R., Aoki, N., Mima, S., Inoue, T., Matsushita, T., 2004. Micro-ground powdered activated carbon for effective removal of natural organic matter during water treatment. Water Sci. Tech.: Water Supply 4 (4), 155–163.

Matsui, Y., Murase, R., Sanogawa, T., Aoki, N., Mima, S., Inoue, T., Matsushita, T., 2005. Rapid adsorption pretreatment with submicron powdered activated carbon particles before microfiltration. Water Sci. Tech. 51 (6–7), 249–256.

Matsui, Y., Aizawa, T., Kanda, F., Nigorikawa, N., Mima, S., Kawase, Y., 2007. Adsorptive removal of geosmin by ceramic membrane filtration with super-powdered activated carbon. J. Water Supply: Res. Technol.–AQUA 56 (6–7), 411–418.

Matsui, Y., Hasegawa, H., Ohno, K., Matsushita, T., Mima, S., Kawase, Y., Aizawa, T., 2009a. Effects of super-powdered activated carbon pretreatment on coagulation and trans-membrane pressure buildup during microfiltration. Water Res. 43 (20), 5160–5170.

Matsui, Y., Ando, N., Sasaki, H., Matsushita, T., Ohno, K., 2009b. Branched pore kinetics model analysis of geosmin adsorption on super-powdered activated carbon. Water Res. 43 (12), 3095–3103.

Najm, I.N., Snoeyink, V.L., Suidan, M.T., Lee, C.H., Richard, Y., 1990. Effect of particle size and background natural organics on the adsorption efficiency of PAC. J. Am. Water Works Assoc. 82 (1), 65–72.

Peel, R.G., Benedek, A., 1980a. Attainment of equilibrium in activated carbon isotherm studies. Environ. Sci. Technol. 14 (1), 66–71.

Peel, R.G., Benedek, A., 1980b. Dual rate kinetic model of fixed bed adsorber. J. Environ. Eng.–ASCE 106 (4), 797–813.

Randtke, S.J., Snoeyink, V.L., 1983. Evaluating GAC adsorptive capacity. J. Am. Water Works Assoc. 75 (8), 406–413.

Sontheimer, H., Crittenden, J.C., Summers, R.S., 1988. Activated Carbon for Water Treatment, second ed. DVGW-Forschungsstelle, Karlsruhe, Germany.

Summers, R. Scott, Hooper, Stuart M., Solarik, Gabriele, Owen, Douglas M., Hong, Seongho, 1995. Bench-scale evaluation of GAC for NOM control. J. Am. Water Works Assoc. 87 (8), 69–80.

Weber Jr., W.J., Voice, T.C., Jodellah, A., 1983. Adsorption of humic substances: effects of heterogeneity and system characteristics. J. Am. Water Works Assoc. 75 (12), 612–619.

WATER RESEARCH 45 (2011) 761–767

Available at www.sciencedirect.com

ScienceDirect

journal homepage: www.elsevier.com/locate/watres

Direct observation of solid-phase adsorbate concentration profile in powdered activated carbon particle to elucidate mechanism of high adsorption capacity on super-powdered activated carbon

*Naoya Ando, Yoshihiko Matsui, Taku Matsushita, Koichi Ohno**

Graduate School of Engineering, Hokkaido University, N13W8, Sapporo 060-8628, Japan

ARTICLE INFO

Article history:
Received 14 March 2010
Received in revised form
27 August 2010
Accepted 30 August 2010
Available online 6 September 2010

Keywords:
SPAC
FIB
SEM
EDXS
Isotherm
PSS
NOM

ABSTRACT

Decreasing the particle size of powdered activated carbon (PAC) by pulverization increases its adsorption capacities for natural organic matter (NOM) and polystyrene sulfonate (PSS, which is used as a model adsorbate). A shell adsorption mechanism in which NOM and PSS molecules do not completely penetrate the adsorbent particle and instead preferentially adsorb near the outer surface of the particle has been proposed as an explanation for this adsorption capacity increase. In this report, we present direct evidence to support the shell adsorption mechanism. PAC particles containing adsorbed PSS were sectioned with a focused ion beam, and the solid-phase PSS concentration profiles of the particle cross-sections were directly observed by means of field emission–scanning electron microscopy/energy-dispersive X-ray spectrometry (FE-SEM/EDXS). X-ray emission from sulfur, an index of PSS concentration, was higher in the shell region than in the inner region of the particles. The X-ray emission profile observed by EDXS did not agree completely with the solid-phase PSS concentration profile predicted by shell adsorption model analysis of the PSS isotherm data, but the observed and predicted profiles were not inconsistent when the analytical errors were considered. These EDXS results provide the first direct evidence that PSS is adsorbed mainly in the vicinity of the external surface of the PAC particles, and thus the results support the proposition that the increase in NOM and PSS adsorption capacity with decreasing particle size is due to the increase in external surface area on which the molecules can be adsorbed.

1. Introduction

Powdered activated carbon (PAC) is used for the treatment of drinking water because this versatile adsorbent removes a broad range of organic pollutants, including pesticides and other organic chemicals, taste and odor compounds, cyanobacterial toxins, and total organic carbon (Suffet and McGuire, 1980; World Health Organization, 2006). Although activated carbon is widely used, it is expensive, and the higher the grade and quality of the activated carbon, the greater its cost (Babel and Kurniawan, 2003). While attention has been focused on investigation of various replacements for activated carbon, enhancing its adsorption has also been studied. For example, reducing the particle size of activated carbon increases the rate of adsorbate uptake and thereby reduces the amount of activated carbon required (Randtke and Snoeyink, 1983; Najm

* *Corresponding author.* Tel./fax: +81 11 706 7280.
E-mail address: matsui@eng.hokudai.ac.jp (K. Ohno).
0043-1354/$ – see front matter © 2010 Elsevier Ltd. All rights reserved.
doi:10.1016/j.watres.2010.08.050

et al., 1990; Jia et al., 2005; Matsui et al., 2005, 2009,); therefore, pulverizing activated carbon has been used as a strategy for cost reduction. Although decreasing the particle size increases the adsorption rate, it has been long assumed that the adsorption capacity does not change with particle size (Randtke and Snoeyink, 1983; Najm et al., 1990). However, several studies have shown that activated carbon with a small particle size (e.g., 100/200 US sieve size, Weber et al., 1983; and 0.73 μm median diameter, Ando et al., 2010) has a higher adsorption capacity for NOM. This NOM adsorption capacity increase is explained by means of a mechanism whereby NOM is adsorbed more in the shell region close to the external surface of the particles than in the region inside the particles because NOM forms aggregates in activated carbon pores and does not fully penetrate the carbon particle (Ando et al., 2010), and a shell adsorption model (SAM) based on this mechanism is proposed and verified by means of adsorption isotherm data (Matsui et al., submitted for publication).

The radial profile of adsorbate concentration throughout a particle, however, has not been confirmed by direct observation. Generally, activated carbon adsorption data is interpreted on the basis of measurement of the adsorbate concentration in the bulk water phase, and the solid-phase concentration profile inside activated carbon particles has rarely been observed. Ahn et al. (2005) recently used microprobe laser-desorption laser-ionization mass spectroscopy to spatially resolve the intraparticle concentration profile within several granular adsorbents, including granular activated carbon particles (40 μm). The study demonstrated the complexity of the intraparticle diffusion process.

The objective of the current study was to directly observe the solid-phase adsorbate concentration profiles of PAC particles and thus verify the shell adsorption mechanism. PAC particles containing PSS as a model adsorbate were sectioned with a focused ion beam (FIB), and the intraparticle solid-phase concentration profiles were directly quantified at a 0.4-μm scale by means of energy-dispersive X-ray spectrometry (EDXS) in a field emission–scanning electron microscope (FE-SEM).

2. Materials and methods

2.1. Adsorbents and adsorbate

Commercially available PAC (Taikou-W, Futamura Chemical Industries Co., Gifu, Japan) was used as received (designated PAC-T) or pulverized in a bead mill (Metawater Co., Tokyo, Japan) to produce super-powdered activated carbon (SPAC) samples of various particle sizes, designated SPACa-T, SPACb-T, SPACc-T, and SPACd-T in order of increasing particle size. A slurry of each activated carbon sample was prepared in pure water and stored at 4 °C before use. The median particle diameters of the samples were 0.7 μm for SPACa-T, 1.1 μm for SPACb-T, 1.9 μm for SPACc-T, 3.0 μm for SPACd-T, and 11.8 μm for PAC-T (as determined with an LA-700 size distribution analyzer, Horiba, Kyoto, Japan). The sulfur content of PAC-T was determined by combustion (International Organization for Standardization, 1998; TOX-100, Mitsubishi Chemical Analytech Co., Mie, Japan) and ion chromatography (DX-120, Dionex Corp., California, USA). PSS (Polymer Standard Service, Mainz, Germany; Mw = 1100 Da; Mw/Mn < 1.2) was used as a model adsorbate (Matsui et al., submitted for publication).

2.2. Preparation of PSS solutions and measurement of adsorption isotherms

PSS solutions (initial concentrations, 4.7 and 104 mg/L) were prepared by dissolving PSS in sulfate-ion-free water containing $NaHCO_3$ (20 mg/L as alkalinity) and $CaCl_2$ (4.9 mg/L as Ca). The PSS solutions were adjusted to pH 7.0 ± 0.1 by the addition of HCl or NaOH as required, and the solutions were filtered through 0.2-μm PTFE (Polytetrafluoroethylene) membrane filters before being used for adsorption isotherm tests. The bottle-point technique was used to conduct the adsorption isotherm tests. Various amounts of activated carbon were added to the PSS solution with efficient mixing, and 125 mL aliquots from the solution containing PSS and activated carbon were transferred to 125 mL vials. The vials were then agitated on a shaker for 3 weeks. After the contents of the vials were filtered through a 0.2-μm PTFE membrane filter, the liquid-phase PSS concentrations were measured. The PSS concentrations were determined by UV absorption at a wavelength of 262 nm (UV-1700, Shimadzu Co., Kyoto, Japan) with a calibration line.

2.3. Solid-phase PSS concentration profile in a PAC-T particle

2.3.1. Preparation of PAC-T samples

To prepare PAC-T particles with adsorbed PSS (PSS-loaded PAC-T), we conducted batch adsorption in a 125 mL vial containing a suspension of PSS (103 mg/L), PAC-T (20 mg/L), $NaHCO_3$ (0.2 mmol/L), and $CaCl_2$ (0.12 mmol/L). Because the PAC concentration profiles were determined by means of EDXS analysis of the sulfur in PSS, no sulfate-ion was added. To prepare PAC-T particles without PSS (blank PAC-T), we conducted a blank test without PSS in a 125 mL vial containing a suspension of PAC-T (20 mg/L), $NaHCO_3$ (0.2 mmol/L), and $CaCl_2$ (0.12 mmol/L). After the vials were shaken for 3 weeks, the PAC-T particles were recovered from the vials by means of centrifugal separation (1000 rpm, 190 *g*, 10 min). The particles were dried for 24 h at about 40 °C.

2.3.2. FIB sectioning of PAC-T particles

PAC-T particles were placed on a silicon (Si) wafer that was mounted with double-stick carbon tape (Nisshin EM Co., Tokyo, Japan) on the specimen holder of the FIB system (FB-2100, Hitachi, Ltd., Tokyo, Japan). After desiccation at 40 °C, the sample surface was coated with a 20-nm layer of platinum (Pt) to avoid charge-up effects by means of ion sputtering equipment (JEC-1600, JEOL, Ltd., Tokyo, Japan). A PAC-T particle was selected arbitrarily during real-time scanning-ion microscope imaging, and tungsten (W) was FIB-deposited on the particle for 20 min to prevent damage to the PAC-T particle during FIB milling, which was performed at a beam energy of 40 kV (Fig. 1a). Deep trenches were grooved around the PAC-T particle by means of gallium (Ga) FIB milling such that a small cubic portion (micro-sample) of the Si wafer with the PAC-T particle on top remained; a corner of the small cubic portion (micro-bridge) was left to connect the micro-sample to the Si

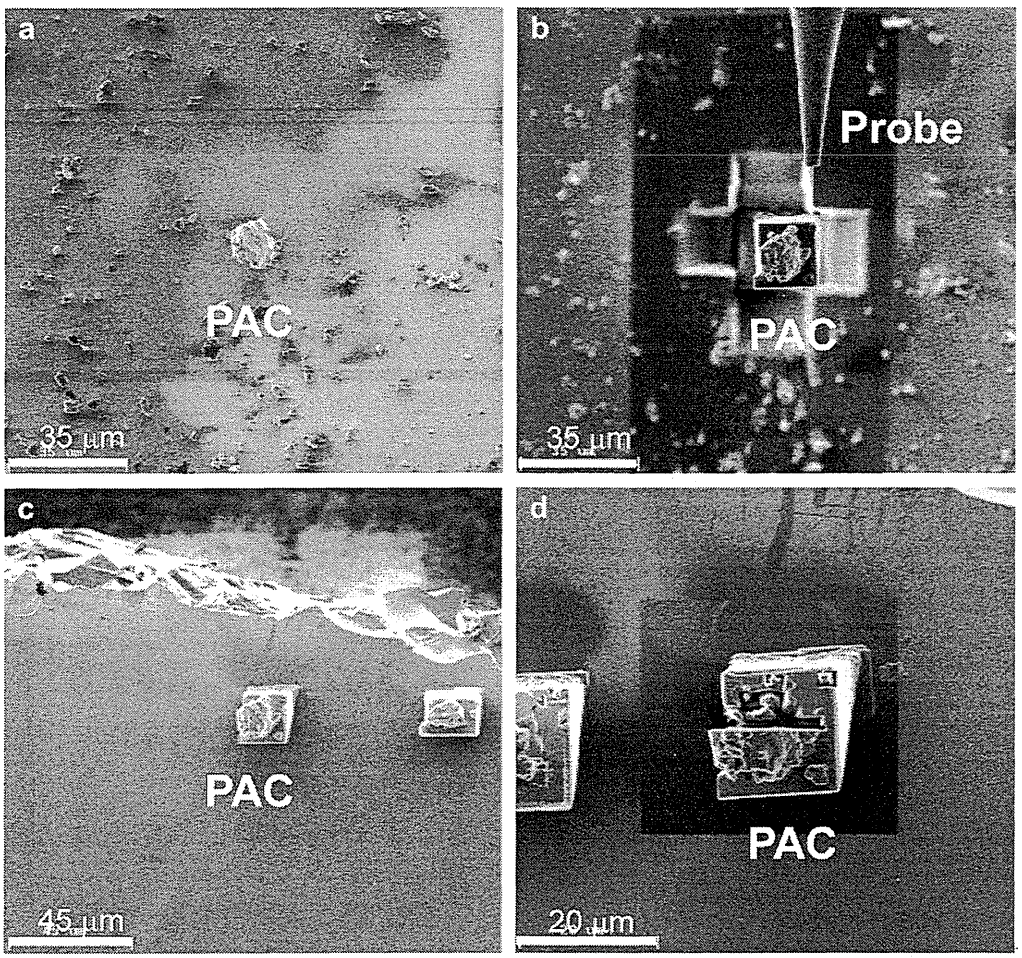

Fig. 1 – Micro-sampling and sectioning of a PAC-T particle using FIB: (a) PAC particles on silicon wafer; (b) micro-sample (small cube with a PAC particle on top) and a tungsten probe; (c) micro-samples on Si wafer, and (d) cross-section of PAC particle.

wafer. Subsequently, the specimen holder was tilted to 60°, and the bottom of the micro-sample was cut with a Ga FIB; as a result, the micro-sample was supported by a micro-bridge at one corner. A mechanical probe was inserted, and the tip of the probe was welded to the micro-sample by means of FIB-assisted W deposition (Fig. 1b). After the micro-bridge was cut with a Ga FIB, the micro-sample was separated from the Si wafer and placed on a newly inserted Si wafer by means of W deposition (4 min). The mechanical probe was cut with a Ga FIB (Fig. 1c) after the newly inserted wafer was mounted on the sample holder of the FIB system by double-stick carbon tape. About half of the PAC-T particle on the micro-sample was then cut away with a Ga FIB to leave a cut PAC-T particle (Fig. 1d). The cut particle was coated with a 2 nm layer of Pt by ion sputtering to avoid charge-up effects during SEM.

2.3.3. *FE-SEM/EDXS of a PAC-T particle*

The Si wafer with the FIB-cut PAC-T particle was mounted with double-stick carbon tape on an L-shaped holder (JEOL) for FE-SEM (JSM-7400F, JEOL) observation of the cross-section of the particle. EDXS line-scan chemical analysis was performed in 0.047-μm increments on the surface of the cross-sectioned particle in the FE-SEM (acceleration voltage, 10 kV; number of sweeps, 25; dwelling time, 0.1 s; magnification, 10,000; working distance, 8.0 mm; JED-2300, JEOL). The penetration depth of electron for the EDXS analysis could be considered large (Castaing, 1960). Lee et al. (2006)

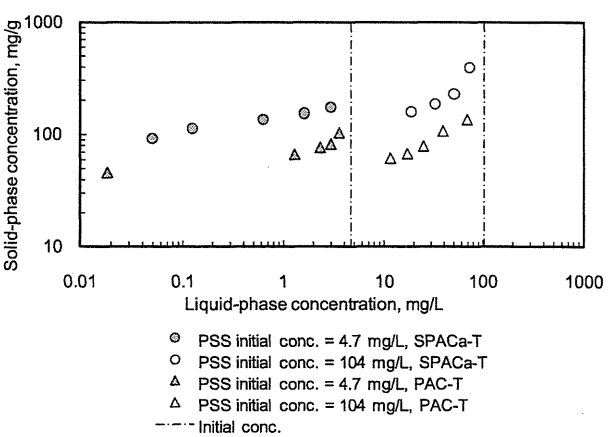

Fig. 2 – Adsorption isotherms of PSS.